GEOLOGICA CARPATHICA, AUGUST 2020, 71, 4, 343–360 https://doi.org/10.31577/GeolCarp.71.4.4

Zirconian–niobian titanite and associated Zr-, Nb-, REE-rich accessory minerals: Products of hydrothermal overprint of leucocratic teschenites (Silesian Unit, Outer Western Carpathians, Czech Republic)

KAMIL KROPÁČ[1,✉], ZDENĚK DOLNÍČEK[2], PAVEL UHER[3], DAVID BURIÁNEK[4], AMINA SAFAI[1] and TOMÁŠ URUBEK[5]

[1]Department of Geology, Faculty of Science, Palacký University, 17. listopadu 12, 771 46 Olomouc, Czech Republic; ✉kamil.kropac@upol.cz
[2]Department of Mineralogy and Petrology, National Museum, Cirkusová 1740, 193 00 Prague 9, Czech Republic
[3]Department of Mineralogy and Petrology, Faculty of Natural Sciences, Comenius University, Ilkovičova 6, 842 15 Bratislava, Slovakia
[4]Czech Geological Survey, Leitnerova 22, 658 59 Brno, Czech Republic
[5]BIC spol. s r. o. Brno: building of the Technology Innovation Transfer Chamber, Purkyňova 125, 612 00 Brno, Czech Republic

(Manuscript received January 23, 2020; accepted in revised form June 12, 2020; Associate Editor: Peter Bačík)

Abstract: Sills of hydrothermally altered alkaline magmatic rock (teschenite) of Lower Cretaceous age at the Čerťák and Řepiště sites in the Silesian Unit (Flysch Belt of the Outer Western Carpathians, Czech Republic) host leucocratic dykes and nests which contain accessory minerals enriched in Zr, Nb and REE: Zr-, Nb-rich titanite, zircon, gittinsite, pyrochlore, monazite, REE-rich apatite, epidote, and vesuvianite. Titanite forms wedge-shaped crystals or irregular aggregates enclosed in the analcime groundmass or overgrowths on Zr-rich ferropargasite and taramite or Zr-rich aegirine–augite to aegirine. Titanite crystals show oscillatory or irregular patchy to sector zoning and contain up to 17.7 wt. % ZrO_2 and 19.6 wt. % Nb_2O_5, and ≤1.1 wt. % REE_2O_3. High-field-strength elements (HFSE) are incorporated into the structure of the studied titanite predominantly by substitutions: (i) $^{[6]}Ti^{4+} \leftrightarrow {}^{[6]}Zr^{4+}$; (ii) $^{[6]}Ti^{4+} + {}^{[6]}Al^{3+} \leftrightarrow {}^{[6]}Zr^{4+} + {}^{[6]}Fe^{3+}$; and (iii) $^{[6]}2Ti^{4+} \leftrightarrow {}^{[6]}Nb^{5+} + {}^{[6]}(Al, Fe)^{3+}$. Magmatic fractional crystallization, high-temperature hydrothermal autometasomatic overprint and low-temperature hydrothermal alterations resulted in the formation of the HFSE-rich mineral assemblages within the leucocratic teschenites. Autometamorphic processes caused by high-temperature hypersaline aqueous solutions (salinity ~50 wt. %, ~390–510 °C), which were released from the HFSE-enriched residual melt, played a major role in the crystallization of Zr-, Nb-, and REE-rich minerals. The mobilization of HFSE could have occurred either by their sequestration into a fluid phase exsolved from the crystallizing melt or by superimposed alteration processes. The distinctive positive Eu anomaly ($Eu_{CN}/Eu^* = 1.85$) of leucocratic dykes infers possible mixing of Eu^{2+}-bearing magmatic fluids with more oxidized fluids.

Keywords: Outer Western Carpathians, Silesian Unit, hydrothermal alteration, teschenite, HFSE, Zr- and Nb-rich titanite.

Introduction

Titanite, $CaTi(SiO_4)O$ is a characteristic accessory mineral in alkaline silicate rocks and, in certain cases, also an important carrier of high-field-strength (HFSE) including rare earth (REE) elements. Individual HFSE, REE and other elements enter different structural positions in titanite: generally, Al^{3+}, Fe^{3+}, V^{3+}, V^{4+}, Nb^{5+}, Ta^{5+}, Sn^{4+}, Zr^{4+}, and Hf^{4+} occupy predominantly the octahedral *Y* (Ti) site, whereas Na^+, Fe^{2+}, Mn^{2+}, REE^{3+}, U^{4+}, and Th^{4+} enter the 7-fold coordinated *X* (Ca) site representing cavities between SiO_4 tetrahedra and TiO_6 octahedra (e.g., Speer & Gibs 1976; Schosnig et al. 1994; Perseil & Smith 1995). Large elemental variations predicate the possible scientific significance of titanite in geology. For instance, U- and Th-bearing titanite can serve as geochronometer (e.g., Storey et al. 2006; Jiang et al. 2016; Hu et al. 2017; Matýsek et al. 2018; Brunarska & Anczkiewicz 2019), the REE contents can provide information about various igneous processes including evolution of the source magma (O'Neill & Eggins 2002; Prowatke & Klemme 2005, 2006; Jiang et al. 2016; Hu et al. 2017; etc.), Nb/Ta ratios are used as indicators of crystal fractionation (e.g., Wolf 1984), and finally, Zr contents can be used to derive geothermometry (Hayden et al. 2008; Cao et al. 2015) or mobility during hydrothermal alteration (Gieré 1990; Rubin et al. 1993; Jiang et al. 2005; Salvi & Williams-Jones 2006; Borst et al. 2016; Marks & Markl 2017).

Titanites with elevated contents of Zr (and usually also Nb and/or REE) are generally rare in nature (Liferovich & Mitchell 2005). Their occurrence is mostly restricted to late derivatives of alkali-rich silica-undersaturated rocks, namely nepheline syenites (Smith 1970; Woolley et al. 1992; Dawson et al. 1995; Vuorinen & Hålenius 2005; Liferovich & Mitchell 2005), and sodalite syenites (Della Ventura et al. 1999) or products of their metasomatic alteration (Reguir et al. 1999). Occurrences of Zr-rich and simultaneously Nb-rich titanite are also known from saturated igneous rocks, such as

trachyandesitic xenoliths in leucocratic tuffs (Gianetti & Luhr 1983), diorite dykes hosted by granite (McLeod et al. 2011) or various types of lamprophyres (Seifert & Kramer 2003; Carlier & Lorand 2008). To date the highest contents of Zr in titanite (15.3 wt. % of ZrO_2; i.e., 0.26 apfu Zr) were discovered in silicocarbonatite from the Afrikanda alkaline–ultramafic complex (Chakhmouradian et al. 2003; Chakhmouradian 2004). The highest content of Nb (16.7 wt. % of Nb_2O_5; i.e., 0.26 apfu Nb) in titanite was recorded in leucotonalitic pegmatite in serpentinized lherzolite from the Staré Město Unit (Bohemian Massif, Czech Republic; Novák & Gadas 2010; Gadas 2012). Similarly high contents of Nb (16.2 wt. % of Nb_2O_5; i.e., 0.25 apfu Nb) are found in titanite related to a zeolite vein in kalsilite-to-nepheline syenite from Mt. Rasvurnchorr in the Khibina massif (Kola Peninsula, Russia; Liferovich & Mitchell 2005). The Zr- and/or Nb-rich titanite often occurs in paragenesis with other Zr-, Nb- or REE-rich accessory minerals, such as zircon and allanite (e.g., Seifert 2005), zirconolite (Della Ventura et al. 1999; Carlier & Lorand 2008), perrierite and baddeleyite (Carlier & Lorand 2008), pyrochlore (Chakhmouradian 2004) or betafite (Liferovich & Mitchell 2005).

In this paper we present new evidence of titanite with high contents of Zr and Nb and elevated contents of REE, occurring in association with other HFSE- and REE-rich accessory minerals (zircon, gittinsite, pyrochlore, monazite, REE-rich apatite, epidote, and vesuvianite) in leucocratic dykes and nests hosted by the hydrothermally altered rocks of teschenite association in the Sub-Beskydy alkaline magmatic province in the Silesian Unit, Outer Western Carpathians (Czech Republic). Until now, detailed studies concerning HFSE and REE minerals in these rocks are sparse. Accessory Zr- Nb-rich titanite (≤14.5 wt. % ZrO_2 and ≤4.4 wt. % Nb_2O_5) in association with zircon, Zr-rich pyroxene and amphiboles (aegirine, katophorite and taramite), and Zr-enriched (hydro)garnets were previously described from syenite dykes in teschenite at Puńców sill, Poland (Włodyka 2007). Other accessory phases found in teschenites include REE-rich apatite-supergroup minerals (Kynický et al. 2009; Kropáč et al. 2017), pyrochlore (Schuchová 2016), Nb-rich baddeleyite, chevkinite-(Ce), and perrierite-(Ce) (Matýsek et al. 2018) and secondary bastnäsite-(Ce), synchysite-(Ce), rhabdophane-(Ce), rhabdophane-(La), cerianite-(Ce), and wakefieldite-(Ce) (Matýsek 2013). Our work represents the first complex mineralogical-geochemical study of Zr-, Nb- and REE-rich mineral association in the rocks of the teschenite association. We attempt to clarify the origin of Zr-, Nb-rich titanite and associated accessory minerals and also try to contribute to the understanding of HFSE and REE partitioning and mobility under hydrothermal conditions.

Regional geology

The studied magmatic rocks of the teschenite association are restricted to the Silesian Unit, which is a part of the Flysch Belt of the Outer Western Carpathians (southern Poland, NE part of the Czech Republic and northern Slovakia; Fig. 1). The Flysch Belt can be subdivided into the Magura and Silesian–Krosno groups of nappes (e.g., Plašienka 1997; Froitzheim et al. 2008), which are interpreted as remnants of several sedimentary basins developed on the margin of the European platform and incorporated into the Carpathian accretionary wedge. The Silesian Unit belongs to the Silesian–Krosno

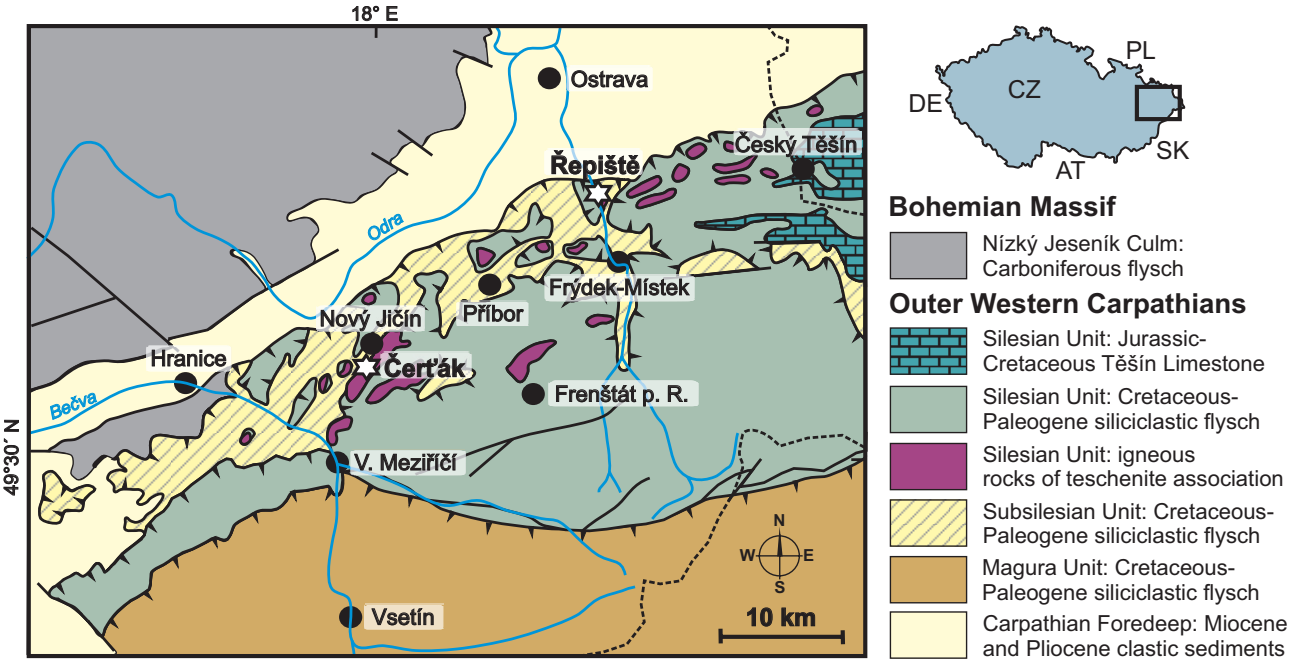

Fig. 1. Geological position of the Čerťák and Řepiště sites in the Outer Western Carpathians nappe system.

Group of nappes and consists mainly of marine sediments of Upper Jurassic to Upper Oligocene age. The base of the rock sequence is characterized by sedimentation of limestones and calcareous mudstones (Oxfordian–Berriasian). Rhythmic and cyclic flysch sedimentation of mudstones and sandstones with sporadic occurrences of conglomerates, dark silicites and pelosiderites started in the Valanginian (Eliáš 1970; Stráník et al. 1993). The emplacement of alkaline magmatic rocks of the teschenite association in the form of hypabyssal sills, submarine extrusions, pillow lavas and volcanoclastic rocks was co-eval with the sedimentation of the Hradiště Formation (Stráník et al. 1993; Eliáš et al. 2003). Isotope whole-rock K–Ar, Ar–Ar and mineral U–Pb dating indicate a Valanginian to Aptian age (~140–120 Ma) of the teschenite magmatism in the Silesian Unit (Lucińska-Anczkiewicz et al. 2002; Grabowski et al. 2003; Szopa et al. 2014; Matýsek et al. 2018; Brunarska & Anczkiewicz 2019). Consequently, this alkaline magmatism was related to early rifting (Narebski 1990; Spišiak & Hovorka 1997; Brunarska & Anczkiewicz 2019) or to reactivation of deep faults during the Lower Cretaceous (Dostal & Owen 1998). The entire teschenite rock sequence was subsequently folded and thrusted towards the NW, onto the SE part of the Bohemian Massif, during the Alpine orogenic event in Miocene (Stráník et al. 1993).

Characterization of teschenite magmatic rocks

Rocks of the teschenite association represent a specific group of alkaline to sub-alkaline igneous rocks ranging from ultrabasic (ultramafic) picrites to intermediate (leucocratic) teschenites. Their wide variability in texture, mineral and chemical composition is mostly explained in terms of various degrees of partial melting of asthenospheric mantle, mixing of magmas of different origins, fractional crystallization, assimilation of crustal rocks, and post-magmatic hydrothermal alteration (Mandour 1982; Kudělásková 1987; Hovorka & Spišiak 1988; Matýsek 1989; Dostal & Owen 1998; Dolníček et al. 2010a,b; Kropáč et al. 2015; Brunarska & Anczkiewicz 2019). The Nd, Sr, and Hf isotopic composition and variations in REE and HFSE suggest that these rocks are a product of ~2–6 % partial melting of upper mantle garnet peridotite at a depth ~60–80 km. This product was compositionally similar to ocean island basalts (OIB) with HIMU (*high*-μ; $\mu = {}^{238}U/{}^{204}Pb$) affinities (Dostal & Owen 1998; Harangi et al. 2003; Brunarska & Anczkiewicz 2019) and could be modified by mixing with the more depleted, MORB-type component (Harangi et al. 2003; Brunarska & Anczkiewicz 2019). Teschenites *sensu stricto* are considered the most felsic and alkaline members of the entire teschenite rock suite. They have generally elevated contents of HFSE (especially P, Ti, Zr, Nb) and LREE, whereas contents of Mg and compatible trace elements (mainly Ni, Cr, V) are low relative to least evolved ultramafic picrites. According to their mineral composition, melanocratic to mesocratic teschenites *s.s.* can be classified as foid gabbro, foid monzogabbro and foid monzosyenite (Pacák 1926; Smulikowski 1930, 1980; Matýsek & Jirásek 2016; Brunarska & Anczkiewicz 2019). Leucocratic types of the teschenites compositionally correspond to foid-bearing alkali-feldspar syenites or foid syenites (Pacák 1926; Smulikowski 1930; Mahmood 1973). However, their mineral and chemical compositions are usually strongly affected by superimposed hydrothermal alterations (Dolníček et al. 2010a; Kropáč et al. 2017) causing serious classification problems.

Studied occurrences of teschenite rocks

A large variability in mineral and chemical composition can be obvious even within a single teschenite body including two occurrences studied in this work. The Čerťák site (49°33'58"N, 17°59'54"E) is situated near the Čerťák water reservoir, ca. 2 km south of the town of Nový Jičín (Fig. 1). A teschenite sill with a thickness over 30 m is exposed there in several small historical quarries. The sill continues north-east from Čerťák toward the village of Bludovice with a total length more than 2 km. The Řepiště site (49°43'40"N, 18°18'27"E) represents one of the largest outcrops of teschenites in the Silesian Unit (Fig. 1). The sill is exposed in a railway cut ca. 800–1200 m SSE of the Paskov railway station.

Both sills are predominantly composed of fine- to coarse-grained mesocratic (M′=~40–50) pyroxene-amphibole to amphibole–pyroxene teschenites, which often pass into a melanocratic pyroxene-rich variety (Pacák 1926; Šmíd 1978; Kudělásková 1987; Hovorka & Spišiak 1988). In addition to pyroxene (Ti-rich diopside) and amphibole (kaersutite) phenocrysts, these rocks contain variable amounts of biotite (phlogopite), hydroxylapatite, and Ti-rich magnetite surrounded by an analcime–feldspar groundmass, and secondary minerals including chlorite, carbonates, and sulphides (Pacák 1926; Šmíd 1978; Kudělásková 1987; Hovorka & Spišiak 1988; Schuchová et al. 2016). Titanite with common composition (ZrO_2<1 wt. %, Nb_2O_5<2 wt. %) occurs as an accessory mineral. Leucocratic types of teschenites are less common and form ~1–7 cm thick dykes or nests (several cm to dm short, discontinuous swelling streaks) randomly distributed in the mesocratic teschenite (Fig. 2). They are medium- to coarse-grained and consist mainly of plagioclase, alkali feldspars, analcime, and natrolite. The mineral association also includes pyroxene, amphibole, slawsonite, biotite, apatite, prehnite, chlorite, thomsonite (Matýsek & Jirásek 2016; Schuchová 2016; Schuchová et al. 2016), and newly recognized rare accessory minerals, including Zr–Nb-rich titanite and other HFSE-, REE-rich minerals, which are the subject of this study.

Methods

We investigated a total of 20 samples of leucocratic dykes or nests from the Čerťák (Č) and Řepiště (Ř) sites (Fig. 2). We made 80 chemical analyses of titanite, more than 100 analyses of other HFSE- or REE-rich accessories, and more

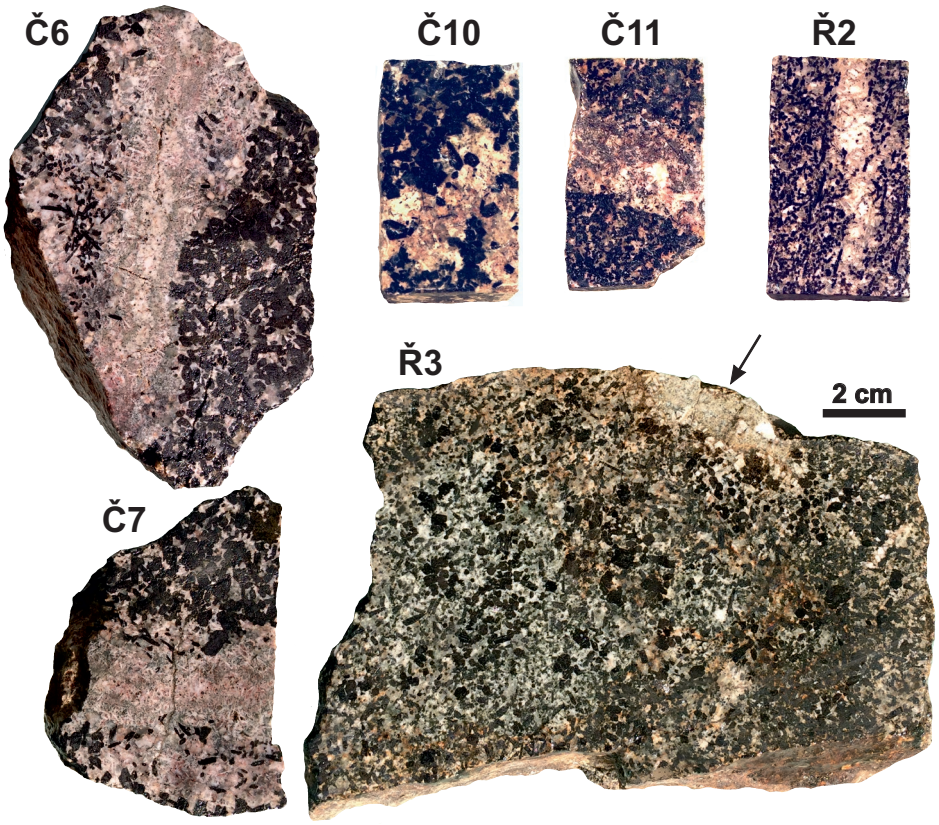

Fig. 2. Macroscopic appearance of selected samples of studied leucocratic dykes (Č6, Č7, Č10, Č11, and Ř2) and nest (Ř3; marked by arrow) hosted by mesocratic pyroxene–amphibole to amphibole–pyroxene teschenites from the Čerťák (Č) and Řepiště (Ř) sites.

than 90 analyses of rock-forming minerals. Electron microprobe analyses were performed using Cameca SX-100 electron microprobes at the Masaryk University in Brno and the National Museum in Prague, Czech Republic. The measurements were carried out on carbon-coated polished thin sections in a wavelength-dispersive mode under the following conditions: acceleration voltage 15 kV, beam current 10 nA, beam diameter 2 μm. The data were converted to wt. % using the automatic PAP procedure (Pouchou & Pichoir 1985). The following analytical lines and standards were used for titanite analyses: *Kα* lines for Na on albite, K and Al on sanidine, Fe on almandine, Mg on pyrope, Ca on wollastonite, Si and Ti on titanite, Sc on $ScVO_4$, and F on topaz; *Lα* lines for Y on YPO_4, Zr on zircon, Nb on columbite, Ta on $CrTa_2O_6$, Sn on Sn, La on $LaPO_4$, and Ce on $CePO_4$; *Lβ* lines for Pr on $PrPO_4$ and Nd on $NdPO_4$; *Mα* lines for Th on synthetic $CaTh(PO_4)_2$.

The empirical formulae were normalized to the sum of 3 cations for titanite, 8 cations for apatite and epidote, 50 cations for vesuvianite, and 2 cations in the *B*-site for pyrochlore supergroup minerals (Atencio et al. 2010). The empirical formulae of zircon and gittinsite were recalculated on the basis of 4 and 7 oxygen atoms, respectively. The Fe^{2+}/Fe^{3+} ratios in epidote and vesuvianite were determined on the basis of the charge balance of the empirical formula. Determination of negative charges in epidote was performed according to the recommendations of Armbruster et al. (2006): Σ (anion charge)=2(12–x)+x+1, where x=F+Cl (apfu). All Fe determined by electron microprobe is considered to be trivalent in titanite and pyrochlore.

The whole-rock chemical analyses were performed in the ACME laboratories (Bureau Veritas, Vancouver, Canada). Major and trace elements were analyzed in samples of the mesocratic host teschenite, a leucocratic dyke and a leucocratic teschenite nest from Řepiště. Samples usually weighing between 0.5 and 1.0 kg were crushed and milled to analytical fineness in an epicyclic mill. The powder was subsequently reduced by quartering to an analytical sample (weighing approximately 10 g). Major oxides and Sc were determined using ICP-ES. Carbon, sulphur and loss on ignition (LOI) were measured with a Leco automatic analyser. The subsamples for heavy metal analyses (Ag, As, Au, Bi, Cd, Co, Cu, Hg, Mo, Ni, Pb, Sb, Se, and Zn) were digested by hot aqua regia (95 °C) and analyzed by ICP-MS. All other elements including REE were analyzed by ICP-MS after melting of another aliquot with $LiBO_2$ and leaching by 5% HNO_3. The trace-element concentrations were normalized to C1-chondrite according to values determined by Barrat et al. (2012). The Ce and Eu anomalies were calculated after the following equations (McLennan 1989; Monecke et al. 2002): $Ce_{CN}/Ce^*=Ce_N/\sqrt{(La_N\times Pr_N)}$; $Eu_{CN}/Eu^*=Eu_N/\sqrt{(Sm_N\times Gd_N)}$.

Results

Mineral association of leucocratic teschenites

The studied leucocratic dykes and nests are fine- to medium-grained, with M´=20–35. They consist mainly of feldspars (~25–50 vol. %) represented by strongly altered relicts of intermediate plagioclase ($An_{36–52}$; Fig. 3a,b), lamellae or irregular grains of newly-formed alkali feldspars (albite $An_{01–02}$ and K-feldspar $Or_{95–99}Ab_{01–05}$; Fig. 3a–c), rarely Ba-rich orthoclase (≤0.12 apfu Ba) and slawsonite (≤0.74 apfu Sr). The feldspars are usually surrounded or corroded by analcime (≤0.26 apfu K) and natrolite, less frequently by thomsonite (Fig. 3c), or locally Sr-rich thomsonite (≤0.27 apfu Sr), which replaces intermediate plagioclase (Fig. 3b). Primary magmatic mafic components are represented mainly by zoned euhedral prismatic diopside (X_{Mg}=0.83–0.96, Ti=0.07–0.10 apfu, Na=0.03–0.04 apfu), amphibole (core: kaersutite or ferrokaersutite: Si=5.63–5.85 apfu, X_{Mg}=0.14–0.62, Ti=0.49–0.61 apfu, Na+K=0.90–0.99 apfu; rim: hastingsite or ferropargasite: Si=5.68–6.11 apfu, X_{Mg}=0.01–0.53, Ti=0.08–0.52 apfu, Na+K= 0.95–1.44 apfu), and tabular biotite (annite: Si=5.32 apfu, Ti=0.60 apfu, Mg=21.5 at. %) phenocrysts (Fig. 3c). These minerals enclose euhedral columnar crystals of fluorapatite (≤2.5 wt. % F), which are frequent also in the surrounding groundmass. The phenocrysts of amphibole are sometimes overgrown by secondary hydrothermal amphibole corresponding to ferropargasite or taramite (Si=5.90–6.51 apfu, X_{Mg}=0.01–0.30, Ti=0.02–0.49 apfu, Na+K= 0.94–1.81 apfu; Fig. 3d) with unusually high contents of Zr (≤6.0 wt. % ZrO_2, 0.50 apfu Zr). Diopside is rimmed by hedenbergite (X_{Mg}= 0.03–0.44) or aegirine–augite to aegirine [J/(Q+J)=0.27–0.95], which is green with sector zoning in plane polarized light. The aegirine–augite to aegirine (Fig. 3d) is also enriched in Zr (≤4.2 wt. % ZrO_2, 0.08 apfu Zr). Biotite (annite to siderophyllite: Si=4.72–6.76 apfu, Mg=1.12–7.52 at. %) sometimes grows on the crystal surface of aegirine–augite to aegirine. Secondary pyroxene, amphibole and biotite with similar characteristics occur also as chloritized columnar or isometric grains in the felsic groundmass (Fig. 3e). Diopside and biotite phenocrysts are often partly or completely altered to a mixture of chlorite, epidote, and titanite. Finally, leucocratic teschenites also contain small amounts of prehnite, chamosite, epidote, calcite, barite, (OH, F)-rich grossular (F≤3.8 wt. %; Fig. 3f), pyrite, Ti-rich magnetite, together with Zr–Nb-rich titanite and other Zr-, Nb-, REE-rich accessory minerals, which are characterized in detail below.

Zr-, Nb-rich titanite

Zirconium- and/or Nb-rich titanite usually forms wedge-shaped crystals or irregular aggregates, up to 100 μm in size. They occur in the analcime groundmass where, in many cases, they grow on amphibole or aegirine–augite to aegirine. Euhedral to subhedral titanite crystals sometimes contain small magnetite or zircon inclusions (Fig. 4a–b) and show patchy to more regular oscillatory zoning in BSE images (Fig. 4a–d). In contrast, anhedral titanite overgrowths on Zr-rich pyroxene and amphibole show irregular patchy to sector zoning (Fig. 4e,f). Brighter zones visible in BSE images contain up to 17.7 wt. % ZrO_2, 19.6 wt. % Nb_2O_5, and 1.1 wt. % REE_2O_3. This corresponds to 0.30 apfu of Zr, 0.32 apfu of Nb, and 0.01 apfu of REE, respectively. The contents of HfO_2 are below 0.5 wt. % (Table 1). Darker zones are poor in the above-mentioned heavier elements and correspond to common titanite widely occurring in the host teschenites. The contents of Ca and Si are mostly similar and close to 1 apfu in the studied titanites. In contrast, Ti, Fe^{3+}, and Al vary between 0.38–0.95, 0.03–0.14, and 0.01–0.27 apfu, respectively. Exceptionally, higher levels of Na (≤0.08 apfu) were recorded. Fluorine in titanite can be as high as 0.19 apfu. The contents of other elements are mostly below 0.01 apfu (Table 1). Titanite spatially related to chlorite pseudomorphs after pyroxene generally contains lesser amounts of HFSE and REE (≤3.4 wt. % ZrO_2, ~0.9 wt. % Nb_2O_5 and ~0.2 wt. % REE_2O_3).

Associated Zr-, Nb-, REE-rich accessory minerals

Besides titanite, the important carriers of Zr in the studied leucocratic teschenites also include zircon and gittinsite. In addition, small amounts of Zr are also hosted by pyrochlore (≤3.4 wt. % ZrO_2), REE-rich epidote (≤1.8 wt. % ZrO_2), and REE-rich vesuvianite (≤0.3 wt. % ZrO_2; Table 2). Zircon forms euhedral to anhedral, small (≤5 μm) crystals enclosed in Zr-rich titanite, analcime, (OH, F)-rich grossular, or limonitized pyrite (Fig. 5a). Anhedral zircon often forms intergrowths with pyrochlore (Fig. 5b). Zircon shows variable contents of Y_2O_3 (0.5–5.2 wt. %, 0.01–0.09 apfu Y) and FeO (≤2 wt. %, ≤0.05 apfu Fe), but is anomalously low in Hf (0.4–0.7 wt. % HfO_2, 0.003–0.006 apfu Hf; $Zr/Hf_{wt.}$=76–135), and generally low in UO_2, ThO_2 and REE_2O_3 (each below ~1 wt. %). There are also local differences in zircon composition; zircons from Čerťák are slightly enriched in Y, U, Th and Ce, compared to those from Řepiště (Table 2). Gittinsite forms irregular overgrowths on chlorite–epidote pseudomorphs after biotite (Fig. 5b). The analyzed gittinsite is almost pure ($Ca_{1.00}Zr_{0.97}Si_{2.00}O_{7.00}$) and corresponds to the ideal formula.

Niobium-bearing minerals are represented by pyrochlore (Fig. 5a–c). It forms grains up to 70 μm in size, usually subhedral with octahedral habitus and uneven fractures (Fig. 5c) or less commonly anhedral irregular grains with slight signs of corrosion. Pyrochlore is enclosed in the felsic groundmass. Rarely, it occurs in association with zircon in the limonitized pyrite (Fig. 5a). Pyrochlore is always rich in Nb (1.04–1.53 apfu) and poor in Ta (below ~0.05 apfu). Both elements occupy the structural position *B* together with Ti (0.26–0.49 apfu), Si (up to 0.37 apfu) and in some cases Zr (up to 0.09 apfu). The structural position *A* is occupied mostly by Ca (0.79–1.06 apfu) and Na (0.18–0.55 apfu) but never completely, with nearly half of the studied pyrochlore analyses showing substantial vacancy ($^{A}\square$=0.42–0.99). Pyrochlore contains up to 0.86 apfu of F.

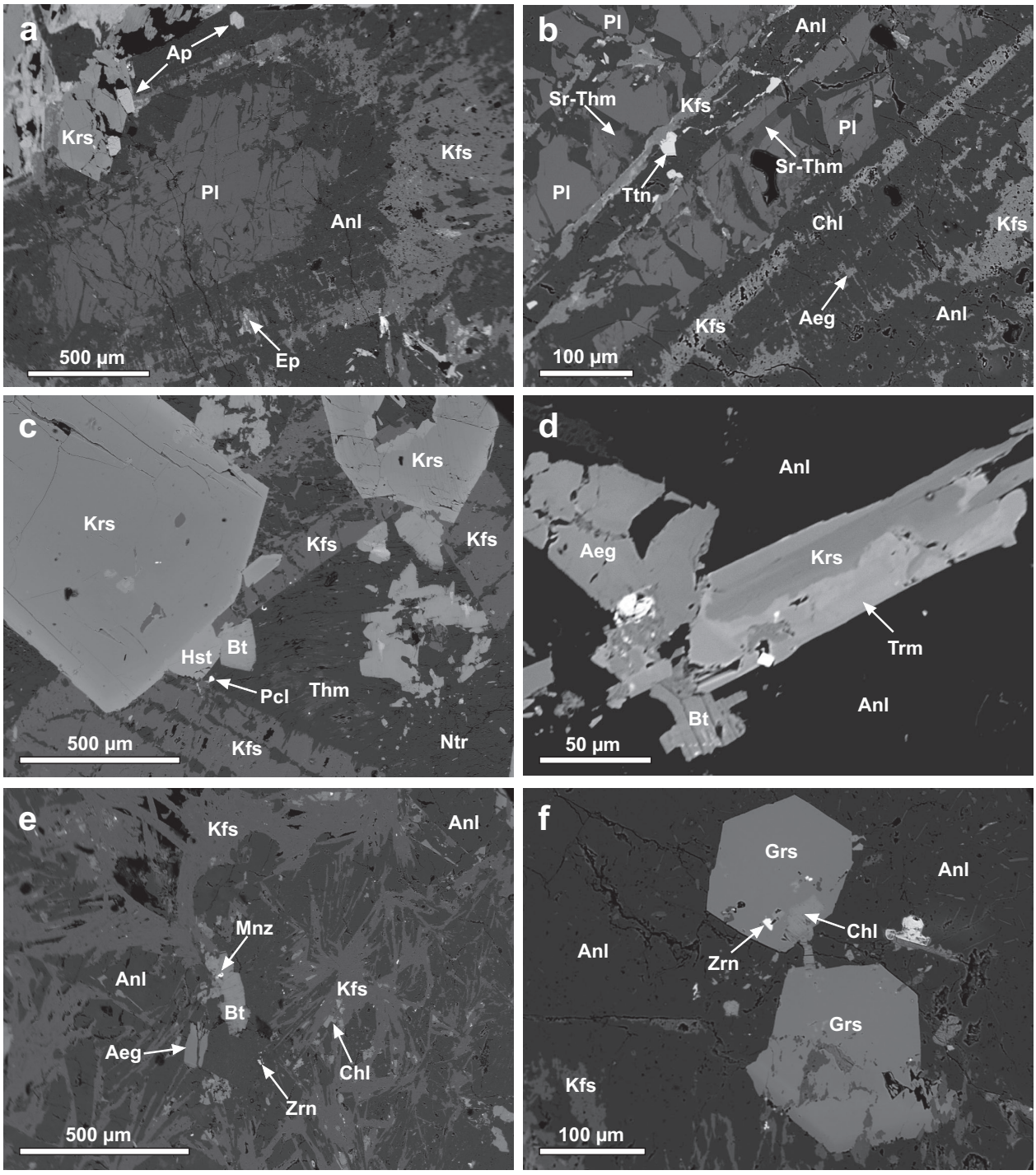

Fig. 3. Mineral association of investigated leucocratic dykes and nests on BSE images: **a** — altered relict of intermediate plagioclase corroded by analcime and secondary K-feldspar (nest Ř3); **b** — slats of intermediate plagioclase partially replaced by newly-formed anhedral alkali feldspars and Sr-rich thomsonite (dyke Ř2b); **c** — primary prismatic kaersutite to ferrokaersutite with hastingsite growth in K-feldspar–zeolite groundmass (dyke Č9); **d** — secondary taramite overgrowing primary ferrokaersutite in association with hydrothermal aegirine-augite to aegirine, annite and analcime (nest Ř3); **e** — secondary aegirine-augite to aegirine and annite to siderophyllite with primary monazite inclusion in the felsic groundmass (nest Ř3); **f** — isometric euhedral grains of (OH, F)-rich grossular enclosing primary zircon inclusion (dyke Ř2b). Mineral abbreviations for Figs. 3–5: Aeg — aegirine–augite to aegirine, Anl — analcime, Ap — apatite, Bt — biotite, Ep — epidote, Grs — grossular, Hst — hastingsite, Chl — chlorite, Git — gittinsite, Kfs — K-feldspar, Krs — kaersutite to ferrokaersutite, Pcl — pyrochlore, Pl — plagioclase, Mgt — magnetite, Mnz — monazite, Ntr — natrolite, Thm — thomsonite, Trm — taramite, Ttn — titanite, Ves — vesuvianite, Zrn — zircon.

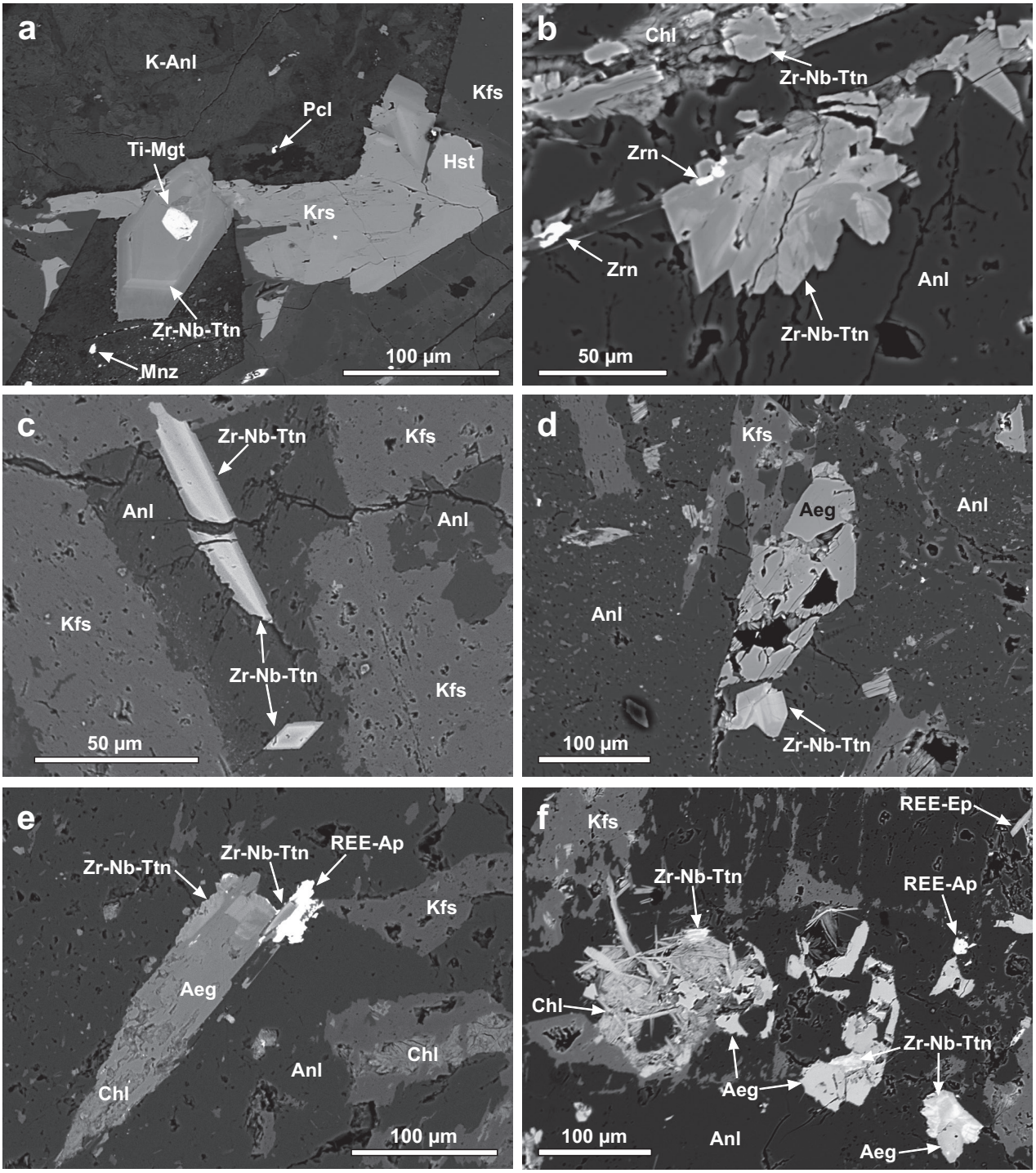

Fig. 4. Morphology and association of Zr-, Nb-rich titanite and other HFSE-rich minerals minerals in BSE images: **a–d** — euhedral to subhedral crystals of Zr-, Nb-rich titanite with oscillatory or irregular patchy to sector zoning and (a) Ti-rich magnetite or (b) zircon inclusions (a — dyke Č10, b — nest Ř3, c — dyke Č7, d — nest Ř3); **e, f** — anhedral growths of Zr-, Nb-rich titanite with irregular patchy to sector zoning on aegirine–augite to aegirine (e — nest Ř3, f — dyke Ř2b). See caption of Fig. 3 for mineral abbreviations.

In addition, lower analytic totals may indicate a presence of molecular water in the structure of pyrochlore or its porosity (Table 2). Consequently, the chemical compositions allow for classification of the pyrochlore mineral as fluorcalciopyrochlore according to IMA nomenclature of the pyrochlore supergroup (Atencio et al. 2010).

The REE-bearing minerals are represented by monazite-(Ce), fluorapatite, epidote, and vesuvianite, in addition to zircon and titanite. Monazite-(Ce) forms up to 100 µm large corroded euhedral crystals or anhedral grains enclosed in annite or analcime. Fluorapatite and epidote form euhedral to subhedral columnar crystals or anhedral irregular grains with

partial dissolution phenomena. They are mostly spatially associated with chlorite and K-feldspar, which constitute pseudomorphs after pyroxene (Fig. 5d), but, in rare cases, they are also enclosed in analcime. The REE-rich fluorapatite (~0.67 apfu F, ≤0.02 apfu REE, ~0.01 apfu Sr) forms small overgrowths on older magmatic hydroxylapatite (Fig. 5e). Epidote is either not zoned or it shows sector zoning. The bulk $Fe^{3+}/(Fe^{3+}+Al)$ ratio varies from 0.18 to 0.48 and the REE contents are as high as 0.31 apfu. Brighter zones in BSE exhibit anomalous enrichment in Sr (≤15.9 wt. % SrO, 0.80 apfu Sr; Table 2), and they are classified as epidote-(Sr) according to Armbruster et al. (2006), because the M3 position is always dominated by Fe^{3+} and the M1 position by Al. Vesuvianite forms up to 70 μm large euhedral to subhedral columnar crystals or crystal aggregates with radial arrangement (Fig. 5f). It is surrounded by natrolite and analcime ground mass. Vesuvianite crystals exhibit sector zoning, and their central parts are relatively enriched in REE (≤0.19 apfu) compared to the rim (Table 2).

Whole-rock composition

The chemical compositions of the mesocratic amphibole–pyroxene host teschenite, the leucocratic teschenite dykes and a leucocratic teschenite nest from Řepiště are shown in Table 3. Contrary to the dyke and nest, the host teschenite contains significantly higher amounts of P_2O_5, TiO_2, Fe_2O_3, MgO and CaO, but lesser amounts of SiO_2, Al_2O_3, Na_2O, and K_2O. The major elements thus reflect higher contents of apatite, Ti-rich diopside, kaersutite, phlogopite, and magnetite and

Table 1: Representative compositions of titanite from leucocratic teschenites (Č — Čerťák, Ř — Řepiště).

Sa./An.	**Č7/58**	**Č10/62**	**Ř1/24**	**Ř1/25**	**Ř2b/99**	**Ř2b/100**	**Ř3/17**	**Ř3/82**	**Ř3/83**	**Ř4/60**
Note	**dyke**	**dyke**	**dyke**	**dyke**	**dyke**	**dyke**	**nest**	**nest**	**nest**	**nest**
Nb_2O_5	3.91	0.76	12.19	10.50	17.34	19.60	1.73	1.39	1.54	0.78
Ta_2O_5	0.32	0.14	0.56	1.02	0.18	0.87	0.24	0.68	0.78	0.24
SiO_2	29.66	30.21	30.05	29.72	28.65	27.60	29.59	28.74	28.48	29.09
TiO_2	31.25	26.29	21.30	22.26	16.08	13.97	25.01	22.36	21.91	24.32
ZrO_2	0.51	4.80	1.44	3.89	1.28	6.51	9.65	15.92	17.69	13.17
HfO_2	na	na	0.28	bdl	na	na	na	na	na	0.13
Al_2O_3	2.07	4.99	4.13	3.52	4.27	2.57	1.71	1.30	1.14	1.63
La_2O_3	0.20	bdl	bdl	bdl	bdl	bdl	bdl	bdl	bdl	bdl
Ce_2O_3	0.51	0.11	0.17	0.18	0.09	0.15	0.09	0.14	0.13	0.21
Pr_2O_3	0.15	bdl	bdl	0.09	bdl	bdl	0.11	bdl	bdl	bdl
Nd_2O_3	0.22	0.09	0.04	bdl	0.06	0.15	bdl	bdl	bdl	0.07
$Fe_2O_3^*$	1.80	1.18	5.13	2.03	5.19	5.17	2.67	1.94	1.86	1.95
CaO	27.58	28.11	24.40	25.92	25.40	21.09	26.63	25.80	25.96	27.55
Na_2O	0.07	bdl	0.68	0.71	0.98	1.82	bdl	0.24	0.20	bdl
K_2O	bdl	bdl	na	na	bdl	bdl	bdl	0.10	0.10	na
F	0.41	1.52	0.20	0.38	0.38	bdl	0.71	bdl	bdl	0.65
O=F	−0.17	−0.64	−0.08	−0.16	−0.16	0.00	−0.30	0.00	0.00	-0.27
Total	98.49	97.61	100.47	100.06	99.74	99.50	97.92	98.61	99.81	99.50
$LREE_2O_3$	1.08	0.20	0.21	0.27	0.15	0.30	0.21	0.14	0.13	0.28
Ca	0.995	1.008	0.884	0.943	0.934	0.812	0.988	0.971	0.975	1.015
La	0.003	bdl	bdl	bdl	bdl	bdl	bdl	bdl	bdl	bdl
Ce	0.006	0.001	0.002	0.002	0.001	0.002	0.001	0.002	0.002	0.003
Nd	0.003	0.001	0.001	bdl	0.001	0.002	bdl	bdl	bdl	0.001
Pr	0.002	bdl	bdl	0.001	bdl	bdl	0.001	bdl	bdl	bdl
Na	0.004	bdl	0.044	0.047	0.066	0.127	bdl	0.017	0.014	bdl
K	bdl	bdl	na	na	bdl	bdl	bdl	0.005	0.005	na
Σ [VII]	1.013	1.010	0.931	0.993	1.002	0.943	0.990	0.995	0.996	1.019
Ti	0.791	0.662	0.542	0.569	0.415	0.377	0.652	0.591	0.578	0.629
Al	0.082	0.197	0.164	0.141	0.173	0.109	0.070	0.054	0.047	0.066
Fe^{3+}	0.046	0.030	0.131	0.052	0.134	0.140	0.070	0.051	0.049	0.050
Nb	0.059	0.012	0.186	0.161	0.269	0.318	0.027	0.022	0.024	0.012
Ta	0.003	0.001	0.005	0.009	0.002	0.008	0.002	0.007	0.007	0.002
Zr	0.008	0.078	0.024	0.064	0.021	0.114	0.163	0.273	0.302	0.221
Hf	na	na	0.003	bdl	na	na	na	na	na	0.001
Σ [VI]	0.989	0.980	1.055	0.996	1.014	1.066	0.984	0.998	1.007	0.981
Si	0.998	1.011	1.015	1.010	0.984	0.991	1.025	1.009	0.998	1.000
F	0.044	0.161	0.021	0.041	0.041	bdl	0.078	bdl	bdl	0.071
Catsum	3.000	3.000	3.000	3.000	3.000	3.000	3.000	3.000	3.000	3.000

na=not analyzed, bdl=below detection limit; *total Fe is given as Fe_2O_3, the contents of Sc_2O_3, V_2O_3, Y_2O_3 and SnO are below detection limits

Table 2: Representative compositions of zircon, gittinsite, pyrochlore, vesuvianite, epidote and apatite from leucocratic teschenites (Č — Čerťák, Ř — Řepiště).

Sa./An.	Č7/52	Ř3/33	Ř3/42	Č9/17	Ř3/45	Č7/54	Č7/55	Č9/25	Č9/36	Ř2b/9
Note	dyke	nest	nest	dyke	nest	dyke	dyke	dyke	dyke	dyke
Mineral	Zircon		Gittinsite	Fluorcalciopyrochlore		Vesuvianite		Epidote	Epidote-(Sr)	Fluorapatite
P_2O_5	bdl	bdl	bdl	na	na	bdl	bdl	bdl	bdl	39.83
Nb_2O_5	na	na	0.32	55.17	44.53	na	na	na	na	na
Ta_2O_5	bdl	na	bdl	0.89	1.51	na	na	na	na	na
SiO_2	31.67	32.19	40.06	0.21	6.76	34.15	34.54	33.12	34.39	0.59
TiO_2	bdl	bdl	0.11	6.25	8.67	1.33	0.87	0.11	0.12	na
ZrO_2	57.27	60.02	39.86	1.82	3.36	0.32	0.09	0.70	bdl	na
HfO_2	0.37	0.69	0.53	na	na	na	na	na	na	na
ThO_2	0.30	0.16	na	0.15	0.12	bdl	bdl	bdl	bdl	bdl
UO_2	0.72	0.14	bdl	0.46	0.79	bdl	bdl	bdl	bdl	na
Al_2O_3	bdl	1.19	0.19	0.07	0.09	16.27	17.37	15.44	15.48	bdl
Y_2O_3	5.18	0.53	bdl	0.12	bdl	0.10	bdl	0.14	bdl	bdl
La_2O_3	bdl	na	na	na	na	0.11	0.08	2.95	bdl	0.14
Ce_2O_3	bdl	na	na	na	na	0.57	bdl	4.81	0.08	0.43
Pr_2O_3	na	na	na	na	na	bdl	bdl	0.47	bdl	bdl
Nd_2O_3	bdl	na	na	na	na	0.10	0.13	1.14	bdl	0.06
Sm_2O_3	bdl	na	na	na	na	bdl	bdl	na	na	na
Dy_2O_3	na	0.13	bdl	na	na	0.12	bdl	bdl	bdl	na
Er_2O_3	na	0.09	bdl	na	na	na	na	na	na	na
Yb_2O_3	na	0.19	na	na	na	na	na	na	na	na
Fe_2O_3	na	na	na	1.93	0.79	7.04	6.57	12.10	20.80	na
FeO	1.99	0.85	0.30	na	na	0.16	0.18	5.70	0.58	0.38
MnO	bdl	na	bdl	bdl	0.10	0.27	0.23	0.43	0.11	bdl
PbO	0.07	na	na	bdl	0.09	bdl	bdl	0.22	bdl	na
MgO	bdl	na	bdl	bdl	bdl	0.08	0.05	0.06	bdl	0.14
CaO	bdl	1.02	18.56	16.09	13.78	34.18	35.56	12.42	12.68	54.53
SrO	na	na	na	na	na	bdl	bdl	8.40	15.93	0.23
Na_2O	na	na	na	4.23	4.85	0.25	0.14	bdl	bdl	bdl
F	bdl	bdl	bdl	4.40	3.42	1.81	1.96	0.29	0.12	2.49
Cl	na	na	na	bdl	bdl	bdl	bdl	bdl	bdl	0.35
O=F+Cl	na	na	na	−1.85	−1.44	−0.76	−0.83	−0.12	−0.05	−1.13
Total	97.57	97.23	99.92	89.93	87.41	96.08	96.95	98.38	100.25	98.04
P	bdl	bdl	bdl	na	na	bdl	bdl	bdl	bdl	2.881
Nb	na	na	0.007	1.534	1.113	na	na	na	na	na
Ta	bdl	na	bdl	0.015	0.023	na	na	na	na	na
Si	1.008	1.006	1.999	0.013	0.374	17.461	17.354	3.017	2.997	0.051
Ti	bdl	bdl	0.004	0.289	0.361	0.512	0.327	0.007	0.008	na
Zr	0.889	0.915	0.970	0.055	0.091	0.080	0.023	0.031	bdl	na
Hf	0.003	0.006	0.008	na	na	na	na	na	na	na
Th	0.002	0.001	na	0.002	0.002	bdl	bdl	bdl	bdl	bdl
U	0.005	0.001	bdl	0.006	0.010	bdl	bdl	bdl	bdl	na
Al	bdl	0.044	0.011	0.005	0.006	9.804	10.288	1.658	1.590	bdl
Y	0.088	0.009	bdl	0.004	bdl	0.027	bdl	0.007	bdl	bdl
La	bdl	na	na	na	na	0.020	0.016	0.099	bdl	0.004
Ce	bdl	na	na	na	na	0.106	bdl	0.161	0.003	0.013
Pr	na	na	na	na	na	bdl	bdl	0.015	bdl	bdl
Nd	bdl	na	na	na	na	0.018	0.023	0.037	bdl	0.002
Sm	bdl	na	na	na	na	bdl	bdl	na	na	na
Dy	na	0.001	bdl	na	na	0.044	bdl	bdl	bdl	na
Er	na	0.001	bdl	na	na	na	na	na	na	na
Yb	na	0.002	na	na	na	na	na	na	na	na
Fe^{3+}	na	na	na	0.090	0.033	2.708	2.483	0.830	1.364	na
Fe^{2+}	0.053	0.022	0.013	na	na	0.068	0.077	0.434	0.042	0.027
Mn	bdl	na	bdl	bdl	0.005	0.118	0.096	0.033	0.008	bdl
Pb	0.001	na	na	bdl	0.001	bdl	bdl	0.005	bdl	na
Mg	bdl	na	bdl	bdl	bdl	0.063	0.035	0.008	bdl	0.017
Ca	bdl	0.034	0.992	1.060	0.816	18.726	19.144	1.213	1.184	4.992
Sr	na	na	na	na	na	bdl	bdl	0.444	0.805	0.012
Na	na	na	na	0.505	0.520	0.244	0.135	bdl	bdl	bdl
F	bdl	bdl	bdl	0.855	0.597	2.933	3.114	0.083	0.034	0.672
Cl	bdl	bdl	na	bdl	bdl	bdl	bdl	bdl	bdl	0.050
Catsum	2.049	2.042	4.003	3.578	3.354	50.000	50.000	8.000	8.000	8.000

na=not analyzed, bdl=below detection limit

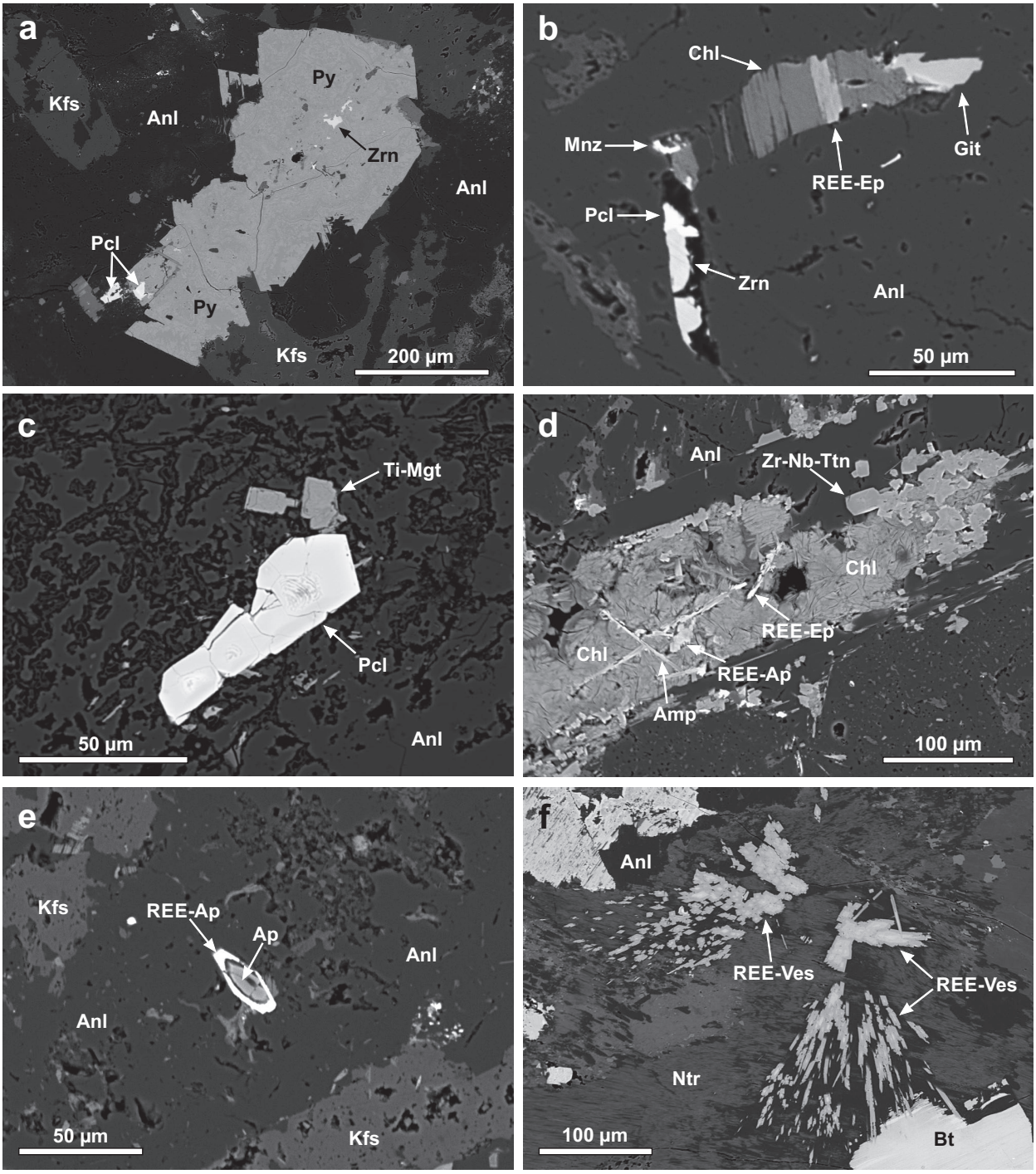

Fig. 5. Morphology and association of gittinsite, pyrochlore and other HFSE- and REE-rich minerals in BSE images: **a** — anhedral zircon and pyrochlore inclusions in the limonitized pyrite (dyke Č7b); **b** — anhedral growths of gittinsite on chlorite and REE-rich epidote pseudomorph after biotite, zircon and pyrochlore grow together on left side of the image (dyke Č7b); **c** — subhedral pyrochlore with octahedral habitus and uneven fractures in analcime groundmass (dyke Č9); **d** — anhedral REE-rich epidote and apatite in chlorite pseudomorph after pyroxene (nest Ř3); **e** — the REE-rich fluorapatite overgrowths on older magmatic hydroxylapatite (nest Ř3); **f** — fan-shaped radial aggregates of REE-rich vesuvianite with sector zoning (dyke Č7b). See caption of Fig. 3 for mineral abbreviations.

lower contents of alkali feldspars and zeolites in the host teschenite. The HFSE are most concentrated in the leucocratic nest, which contains 657 ppm Zr, 179 ppm Nb, 10 ppm Hf, 13 ppm Ta, 34 ppm Th, and 12 ppm U. These values are approximately two to three times higher than those for the host teschenite and leucocratic dyke. The contents of REE (La to Lu+Y) are highest in the host teschenite (354 ppm), whereas leucocratic nest and dyke contain only 285 and 173 ppm,

respectively. Both host teschenite and the dyke have elevated Sr contents (1069–1223 ppm) in comparison to the nest (305 ppm; Table 3).

Discussion

Substitution mechanisms in Zr–Nb-rich titanite

The chemical composition of studied titanites $XY(TO_4)O$ infers that the tetrahedral *T* (Si) site and 7-fold coordinated *X* (Ca) site are almost fully occupied by Si and Ca, respectively. Only a small part of the Ca site is reserved for REE or rarely Na. The octahedral *Y* (Ti) site is predominantly occupied by Ti, Al, Fe^{3+}, Nb, and Zr. Zirconium can substitute on the Ti site of the titanite structure by simple substitution $^{[6]}Ti^{4+} \leftrightarrow {}^{[6]}Zr^{4+}$ (e.g., Sahama 1946; Della Ventura et al. 1999; Chakhmouradian 2004). However, a diagram of Zr vs. Ti (Fig. 6a) clearly illustrates that simple substitution cannot be the only substitution mechanism in our case due to the very low R^2 value of −0.20. Similarly, there is no simple correlation between Zr and (Al, Fe^{3+}) or Zr and Nb (R^2 values are −0.11 and −0.01, respectively). Distinctive negative correlation (R^2=−0.72) in Fig. 6b suggests that the incorporation of Zr into titanite may occur through the coupled substitution: $^{[6]}Ti^{4+} + {}^{[6]}Al^{3+} \leftrightarrow {}^{[6]}Zr^{4+} + {}^{[6]}Fe^{3+}$ (Seifert & Kramer 2003; Cherniak 2006). The involvement of the Al^{3+} and Fe^{3+} minimize lattice distortion and also allows for entry of M^{5+} cations according to the $2\,{}^{[6]}Ti^{4+} \leftrightarrow {}^{[6]}(Nb, Ta)^{5+} + {}^{[6]}(Al, Fe)^{3+}$ mechanism (Clark 1974; Černý et al. 1995; Chakhmouradian 2004; Vuorinen & Hålenius 2005; Pieczka et al. 2017). The relationship between Ti and Nb is shown in Fig. 6c (R^2=−0.38) whereas Fig. 6d illustrates a general relationship between the R^{4+} cations and R^{5+} and R^{3+} cations and the complexity of substitution mechanisms. The incorporation of Na and/or REE in titanites is possible by four coupled substitutions: (1) $2\,{}^{[7]}Ca^{2+} \leftrightarrow {}^{[7]}Na^{+} + {}^{[7]}REE^{3+}$ (Chakhmouradian & Mitchell 1999; Vuorinen & Hålenius 2005; Stepanov et al. 2012), (2) $^{[7]}Ca^{2+} + {}^{[6]}Ti^{4+} \leftrightarrow {}^{[7]}REE^{3+} + {}^{[6]}(Al, Fe)^{3+}$ (Zabavnikova 1957; Vlasov et al. 1964; Lyakhovich 1968; Ribbe 1980; Green & Pearson 1986; Broska et al. 2004; Uher et al. 2019), (3) $2\,{}^{[7]}Ca^{2+} + {}^{[6]}Ti^{4+} \leftrightarrow {}^{[7]}2REE^{3+} + {}^{[6]}Fe^{2+}$ (Ribbe 1980; Gieré 1992; Uher et al. 2019), or (4) $^{[7]}Ca^{2+} + {}^{[6]}Ti^{4+} \leftrightarrow {}^{[7]}Na^{+} + {}^{[6]}(Nb, Ta)^{5+}$ (Sahama 1946; Chakhmouradian & Mitchell 1999). None of these substitutions can be reliably confirmed in our case due to low concentrations of Na and REE in the titanites.

Mobility of HFSE and REE under hydrothermal conditions

Although the HFSE are normally considered to be conservative from the perspective of mobility during hydrothermal process, numerous experimental (e.g., Cherniak 2006; Migdisov & Williams-Jones 2009; Migdisov et al. 2011) and empirical studies (e.g., Kwak & Abbeysinghe 1987; Gieré 1990; Della Ventura et al. 1999; Jiang et al. 2005) document their mobility in hydrothermal solutions under certain

Table 3: Chemical composition of leucocratic vein, nest and host teschenite from Řepiště (oxides, LOI, Tot/C and Tot/S in wt. %, trace elements in ppm, only Au in ppb).

Sample	Ř2a	Ř2b	Ř3
Note	host rock	dyke	nest
P_2O_5	0.88	0.08	0.02
SiO_2	46.37	53.57	54.88
TiO_2	2.62	0.35	0.29
Al_2O_3	16.85	22.44	21.32
Cr_2O_3	<0.002	<0.002	<0.002
$Fe_2O_3^*$	9.93	2.41	2.92
MgO	3.87	0.37	0.17
CaO	7.81	2.39	0.71
MnO	0.18	0.05	0.05
Na_2O	5.46	9.39	8.76
K_2O	2.28	2.71	4.51
LOI	3.30	5.90	6.00
Total	99.67	99.79	99.80
Tot/C	0.03	<0.02	<0.02
Tot/S	<0.02	<0.02	<0.02
LILE			
Rb	46.0	52.9	85.4
Cs	4.4	8.0	5.4
Sr	1069	1223	305
Ba	1125	1336	1128
HFSE			
Th	10.1	10.6	34.1
U	3.4	3.6	12.1
Pb	4.4	5.5	13.7
Nb	118	78.0	179
Ta	6.6	5.1	12.9
Zr	287	242	657
Hf	5.9	3.7	10.2
Y	32	13.1	23.1
REE			
La	77.2	48.1	82.8
Ce	133	71.6	120
Pr	15.5	6.7	10.5
Nd	57.4	19.9	29.6
Sm	10.2	3.1	4.0
Eu	3.3	1.8	0.67
Gd	9.6	2.7	3.5
Tb	1.3	0.42	0.61
Dy	7.1	2.4	3.6
Ho	1.3	0.47	0.84
Er	3.3	1.4	2.7
Tm	0.40	0.20	0.43
Yb	2.4	1.2	2.8
Lu	0.34	0.18	0.39
Sum REE	322	160	262
Ce/Ce*	0.92	0.96	0.97
Eu/Eu*	1.03	1.85	0.54
Other trace elements			
Sc	5.0	<1.0	<1.0
V	168	18.0	14.0
Co	24.0	5.0	5.9
Ni	1.4	0.7	1.2
Cu	16.1	7.2	7.9
Zn	69.0	23.0	28.0
Ga	21.7	21.2	21.5
Mo	1.2	1.1	0.9
Sn	2.0	1.0	4.0
W	1.1	0.9	0.9
Au	1.1	<0.5	1.5

*total Fe is given as Fe_2O_3

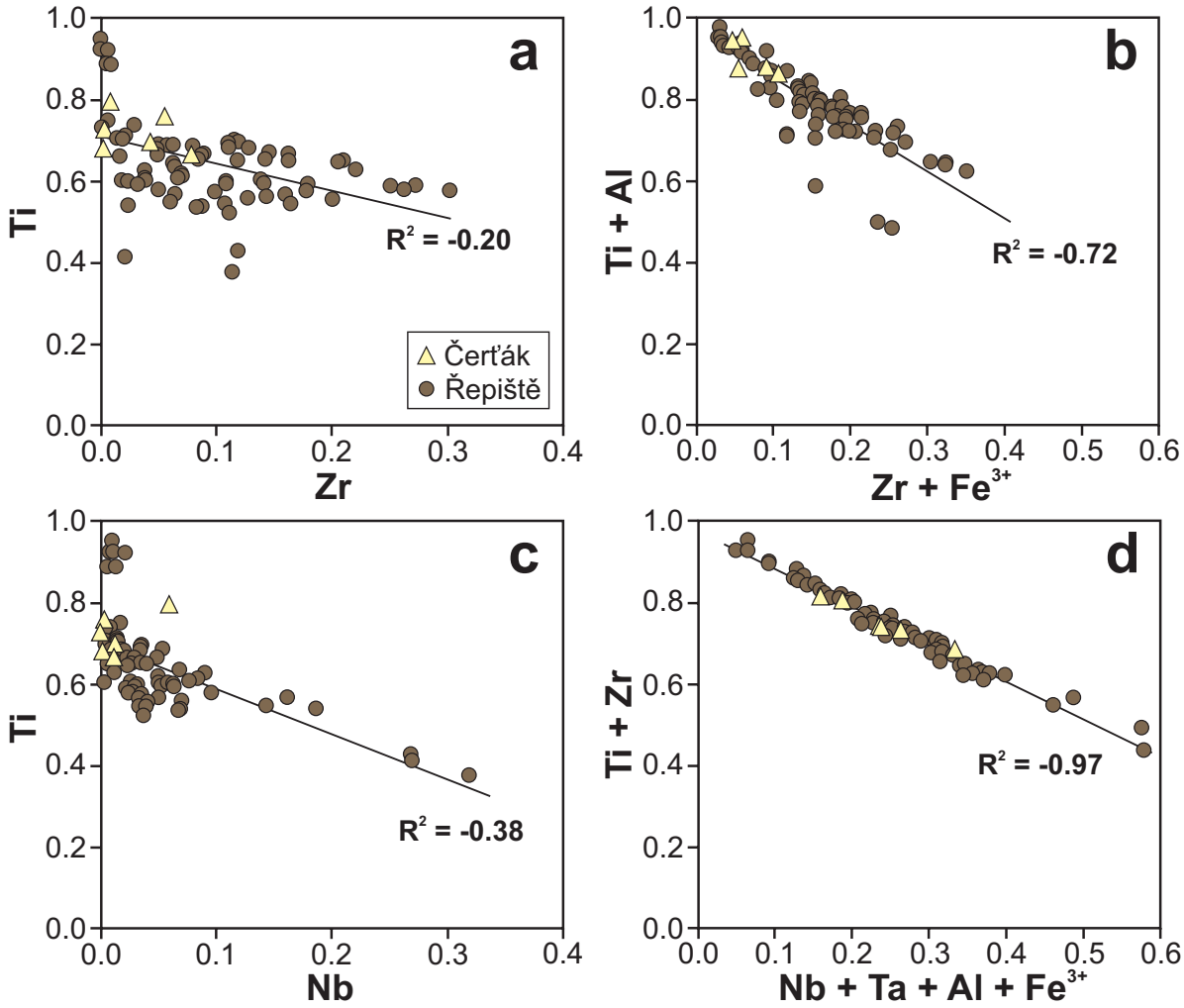

Fig. 6. Substitution diagrams showing the relationships among Zr, Ti, Al, Fe^{3+}, Nb and Ta contents (apfu) in studied titanites.

circumstances. The mobilization of HFSE can be caused by separation of a fluid phase from the melt or by subsolidus alteration processes, involving magmatic, metamorphic or even meteoric fluids. The mobility of Zr, Ti, Nb and other HFSE is controlled by many factors, including P–T conditions, pH, and chemical composition of the fluid phase (Gieré 1990; Rubin et al. 1993; Aja et al. 1995; Salvi et al. 2000; Jiang et al. 2005; Salvi & Williams-Jones 2006; Migdisov et al. 2011; Timofeev & Williams-Jones 2015), and often is enhanced by high activity of dissolved F^- and $(OH)^-$, or possibly $(SO_4)^{2-}$ and $(PO_4)^{3-}$. Similarly, the mobility of REE can be increased by the presence of dissolved Cl^- or other REE-complexing ligands, namely F^-, $(OH)^-$, $(CO_3)^{2-}$, $(SO_4)^{2-}$ and $(PO_4)^{3-}$ (Kraynov et al. 1969; Kwak & Abbeysinghe 1987; Gieré 1990; Della Ventura et al. 1999; Jiang et al. 2005; Salvi & Williams-Jones 2005, 2006; Mitchell & Liferovich 2006; Migdisov & Williams-Jones 2009; Migdisov et al. 2011; Borst et al. 2016). The incorporation of Zr, Nb, and REE from hydrothermal solutions into newly-formed accessory minerals is dependent on many factors including especially changes in temperature and fluid composition, and their precipitation is usually initiated by decrease of temperature in space or time, by changes in fluid composition as a result of precipitation of other phases (Gieré 1990), or by change in salinity due to interaction with the wall rock (Kwak & Abeysinghe 1987).

Although we do not have precise data on the composition of the fluid phase that formed the studied mineral association of the leucocratic teschenites, we can rely on the occurrence and chemical composition of individual minerals and previous research of fluid inclusions in the teschenites. The abundances of fluorapatite (≤5.5 vol. %; Schuchová 2016), fluorcaphite (Kropáč et al. 2017) and Na-minerals (feldspars, zeolites, and aegirine) in the studied teschenites and in associated hydrothermal veins point to relatively high activities of P and Na in the fluids. In addition, the elevated activity of F in hydrothermal fluids associated with teschenites is documented by occurrence of fluorite (Dolníček et al. 2010a) and relatively high contents of F in hydrothermal minerals, ranging from several wt. % in pyrochlore, apatite, titanite, vesuvianite, and (OH, F)-rich grossular to tenths of wt. % in aegirine–augite to aegirine, ferropargasite to taramite, annite, and REE-rich epidote. A fluid inclusion study of non-zoned Zr-poor titanite and

aegirine–augite to aegirine in hydrothermally altered mesocratic pyroxene teschenite from Tichá indicated that these minerals originated from NaCl-rich, $CaCl_2$-poor hypersaline aqueous solutions (salinity of 47–57 wt. %) exsolved during crystallization of the teschenite magma at ~390–510 °C and <100 MPa (Dolníček et al. 2010a). Similar genetic conditions have also been suggested for the high-temperature stage of the Zr–Y–REE–Nb–Be mineralization from the Middle Proterozoic peralkaline pluton at Strange Lake, Quebec, Labrador, where mobilization, transport and deposition of HFSE and REE were mediated by high-temperature (≥350 °C) Na-rich and Ca-poor orthomagmatic fluids (Salvi & Williams-Jones 1996). Other works emphasize the role of F-rich fluids for mobility of HFSE (e.g., Gieré 1990; Della Ventura et al. 1999; Jiang et al. 2005; Migdisov & Williams-Jones 2009; Migdisov et al. 2011). Consequently, we conclude that Na^+, Cl^-, F^-, and $(OH)^-$ were major ligands, which facilitated the mobility of HFSE and REE in hydrothermal fluids.

Origin and evolution of leucocratic dykes and nests

After the emplacement of the teschenite sill and the major phase of fractional crystallization, cracks and pockets filled with residual melt and magmatic fluids developed in the largely solidified igneous body. Leucocratic nests are enriched in U, Th, Nb, Ta, Zr, Hf, La, Yb, and Lu but depleted in other REE, P, and Ti relative to the host pyroxene-amphibole to amphibole–pyroxene teschenite (Fig. 7a). A significant negative Eu anomaly (Eu_{CN}/Eu^*=0.54) of leucocratic nests (Fig. 7b) can reflect the earlier fractionation of Eu^{2+} into plagioclase in lesser evolved teschenite. In contrast, the leucocratic dykes have undergone a different evolution, as illustrated by a depletion in HFSE and REE against the host-rock (Fig. 7a,b) and a distinct positive Eu anomaly (Eu_{CN}/Eu^*=1.84). The depletion in HFSE contents of the leucocratic dykes can be explained in terms of percolation of the leucocratic dyke by external fluids derived from surrounding sediments (i.e., diagenetic and marine waters; Dolníček et al. 2010a, b; Dolníček et al. 2012; Jirásek et al. 2017) enriched in sulphate ions, which have been considered to be important HFSE-complexing ligands (e.g., Gieré 1990; Jiang et al. 2005). Activity of aqueous fluids could also be associated with remobilization of Eu from wall rocks (i.e., Schwinn & Markl 2005) and its subsequent co-precipitations with hydrothermal minerals in the leucocratic dyke giving rise to the observed pronounced positive Eu anomaly of this rock.

Genesis of the HFSE-rich mineral association in leucocratic dykes and nests

The mineral assemblage of leucocratic dykes and nests hosted by teschenites was formed by processes of magmatic fractional crystallization, high-temperature hydrothermal autometamorphic overprint and low-temperature hydrothermal alteration. We can reconstruct the origin and evolution of the mineral association on the basis of textural relationships among individual minerals and their chemical composition.

Magmatic fractional crystallization of rock-forming minerals

Alkaline melts are characterized by high solubility of HFSE (e.g., Watson 1979; Keppler 1993; Linnen & Keppler 2002), and fractional crystallization is considered to be responsible for enrichment of residual melts in HFSE (Wilkinson 1959; Gamble 1984).

The crystallization temperature of the teschenite magma is estimated between ~1200 °C (liquidus) and ~800 °C (solidus) (Wieser 1971). During the main phase of magmatic

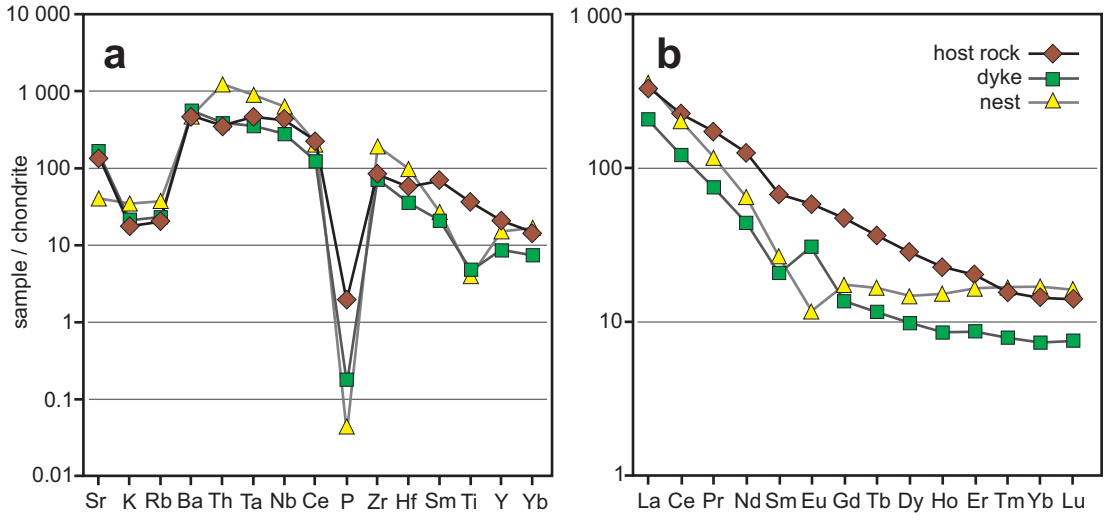

Fig. 7. Chondrite normalized (**a**) LILE and HFSE and (**b**) REE abundance for host mesocratic amphibole–pyroxene teschenite and leucocratic dyke and nest from Řepiště site (samples Ř2a, Ř2b and Ř3). Normalization values are from Barrat et al. (2012).

crystallization, common rock-forming minerals (i.e., apatite, central parts of clinopyroxene, clinoamphibole, and biotite, intermediate plagioclase, and possibly also certain parts of K-feldspar and Ti-rich magnetite) sequentially crystallized from the melt. During this stage, Zr, Hf, U, Th, Y and REE were incorporated into monazite and zircon, which, based on paragenetic evidence, appear to be the oldest HFSE-bearing phases in the studied rocks. The origin of pyrochlore may be either late magmatic or hydrothermal (e.g., Černý & Ercit 1989; Lewandowski et al. 1992; Lumpkin & Mariano 1995; Zurevinski & Mitchell 2004) based on the textural features.

High-temperature hydrothermal autometamorphic overprint

The origin of other Zr-, Nb-, REE-rich accessory minerals present in the studied leucocratic dykes and nests is probably connected with autometamorphic processes, which took place after exsolution of the fluid phase from the crystallizing melt. We conclude that, in this stage, precipitation of Zr-, Nb-rich titanite, aegirine–augite to aegirine and Ca to Na–Ca amphibole occurred, followed by annite. The estimated conditions of crystallization were probably analogous to those suggested by the fluid inclusion study of Dolníček et al. (2010a): high salinity (~50 wt. %), ~390–510 °C, and <100 MPa. Titanite preferentially removes Zr from the hydrothermal solution as the Zr diffusion rate is much faster than those of Sr and the REE (Cherniak 2006). The zoning patterns in titanite also infer a diffusion-controlled growth (Cherniak 2006). Part of the Zr could originate from dissolution of zircon grains. Moreover, titanite could obtain a minor part of Zr also by partial dissolution of Zr-rich aegirine–augite, aegirine, ferropargasite or taramite, which can be broken down more easily than zircon by hydrothermal solutions (Rubin et al. 1993). High Zr content in pyroxenes and amphiboles is a relatively rare phenomenon in nature, and it occurs only in some Zr-rich alkaline magmatic rocks. For example, alkali amphiboles from benmoreites contain up to 4.1 wt. % ZrO_2 (Pearce 1989) and aegirine–augite to aegirine from felsic alkaline rock reveals up to 5.6 wt. % ZrO_2 (Njonfang & Nono 2003). A possible source of Nb and REE in titanite could be older corroded pyrochlore and monazite, respectively.

Also during this stage, precipitation of the REE-rich accessory minerals, vesuvianite and epidote started. Vesuvianite incorporated REE into its structure in the early stages of growth, as shown by its zoning (Fig. 5f). REE-rich vesuvianites are known from altered greenstones from San Benito County in California (Murdoch & Ingram 1966; Crook & Oswald 1979; Fitzgerald et al. 1987) or alkaline magmatic rocks (syenites and nepheline syenites) from Seward Peninsula in Alaska (Himmelberg & Miller 1980) where their origin is connected with metasomatic fluids. In teschenites, vesuvianite is an uncommon mineral phase, but it has been described together with Fe-rich grossular and analcime porphyroblasts in metamorphosed sediments in contact with the teschenite intrusions at the Řepiště and Krmelín sites (Matýsek 1992; Matýsek & Jirásek 2016). A large variability in the occurrence and textural features of epidote implies a wider range of precipitation conditions.

The final stage of high-temperature alteration and transition to the low-temperature hydrothermal evolution was connected with crystallization of prehnite, chlorite, REE-rich apatite, hydrothermal K-feldspar and analcime. Late fluid-related origin of analcime is suggested by many workers (e.g., Kapusta & Włodyka 1997; Włodyka & Kozlowski 1997; Włodyka & Karwowski 2003; Dolníček et al. 2010a). Fluids circulating in the studied teschenite bodies were rich in Na, K, and Ca, but also in Ba and Sr, which further allowed for crystallization of hyalophane and slawsonite (Dolníček et al. 2010a; Matýsek & Jirásek 2016; Schuchová 2016). The REE- and Sr-rich fluorapatite in the groundmass can be correlated with compositionally similar apatite from hydrothermally altered teschenite at Tichá, which was unequivocally proved to be hydrothermal and genetically coeval with analcime (Dolníček et al. 2010a; Kropáč et al. 2017).

Low-temperature hydrothermal alteration

During the further evolution of the rocks, both temperature and salinity of the hydrothermal fluids rapidly decreased, which led to the second alteration, partial remobilization of Sr and HFSE and crystallization of HFSE-enriched minerals (gittinsite, titanite, epidote and fluorapatite) within or in the rim of chlorite pseudomorphs. Gittinsite is a relatively rare Zr mineral described from pegmatitic lenses in a regionally metamorphosed agpaitic syenite (Kipawa complex; Ansell et al. 1980) and has recently been found as an autometasomatic alteration product of eudialyte (Ilímaussaq complex; Borst et al. 2016). Gittinsite crystallizes from low-temperature (≤200 °C) hydrothermal solution under specific circumstances (e.g., Salvi & Williams-Jones 1996). Low-temperature alteration also led to formation of chlorite and albite, and subsequently zeolites (Sr-rich thomsonite and natrolite), carbonates, barite, and pyrite. Based on existing fluid inclusion and isotopic studies of teschenites, a similar mineral association including analcime, chlorite and carbonates was formed from a low-salinity (~0.5–4.5 wt. % of NaCl equiv.) and warm (~190–90 °C) hydrothermal solution (Dolníček et al. 2010a; Urubek et al. 2013). The origin of the fluids was predominantly external, derived from surrounding flysch sediments during diagenetic dehydration of clay minerals (Dolníček et al. 2010a).

Conclusions

Leucocratic nests and dykes hosted by Lower Cretaceous teschenite sills in the Silesian Unit (Flysch Belt of the Western Carpathians, Czech Republic) host numerous accessory HFSE- and REE-rich minerals, with origins largely attributed to hydrothermal processes. The mobilization of HFSE and REE was enabled either by separation of a fluid phase from the melt or by alteration processes involving magmatic fluids

which contain Na^{+} and Zr^{4+}-, Nb^{5+}-, and REE^{3+}-complexing ligands, such as Cl^{-}, F^{-}, and $(OH)^{-}$. The mobilization of HFSE also occurred during low-temperature hydrothermal alteration. A distinctive positive Eu anomaly of leucocratic dykes points to possible mixing of Eu^{2+}-bearing magmatic fluids with more oxidizing fluids derived from outside the magmatic body. Zircon, monazite and perhaps also pyrochlore are considered to be the oldest primary (i.e., magmatic) HFSE and REE carriers in the studied rocks, whereas Zr-, Nb-rich titanite, gittinsite and REE-rich vesuvianite, epidote, and apatite crystallized subsequently during the hydrothermal alteration. The Zr, Nb and REE transported in hydrothermal solution possibly originated from dissolved crystals of older zircon, pyrochlore and monazite, respectively. The Zr-, Nb-rich titanite contains up to 17.7 wt. % ZrO_2 and 19.6 wt. % Nb_2O_5 (both are the highest contents ever reported worldwide) and ≤1.1 wt. % REE_2O_3. HFSE were incorporated into the structure of titanite primarily by the following substitutions: (i) $^{[6]}Ti^{4+} \leftrightarrow {}^{[6]}Zr^{4+}$; (ii) $^{[6]}Ti^{4+} + {}^{[6]}Al^{3+} \leftrightarrow {}^{[6]}Zr^{4+} + {}^{[6]}Fe^{3+}$; and (iii) $^{[6]}2Ti^{4+} \leftrightarrow {}^{[6]}Nb^{5+} + {}^{[6]}(Al, Fe)^{3+}$.

Acknowledgements: This work was supported by the projects IGA_PrF_2017_022 and IGA_PrF_2018_025 (to K.K.) and due to institutional funding from the National Museum as a research organization 00023272 under projects DKRVO 2018/02 and DKRVO 2019-2023/1.II.b (to Z.D.), the Slovak Research and Development Agency under contracts APVV-14-0278, APVV-15-0050, and VEGA Agency No. 1/0499/16 (to P.U.) and Czech Geological Survey research project No. 321180 (to D.B.). We also gratefully thank both reviewers (R. Gieré and R. Škoda) for constructive and helpful comments which improved the clarity of the manuscript.

References

Aja S.U., Wood S.A. & Williams-Jones A.E. 1995: The aqueous geochemistry of Zr and the solubility of some zirconium-bearing minerals. *Appl. Geochem.* 10, 603–620.

Ansell H.G., Roberts A.C., Plant A.G. & Sturman B.D. 1980: Gittinsite, a new calcium zirconium silicate from the Kipawa agpaitic syenite complex, Quebec. *Can. Mineral.* 18, 201–203.

Armbruster T., Bonazzi P., Akasaka M., Bermanec V., Chopin C., Gieré R., Heuss-Assbichler S., Liebscher A., Menchetti S., Pan Y. & Pasero M. 2006: Recommended nomenclature of epidote-group minerals. *Eur. J. Mineral.* 18, 551–567. https://doi.org/10.1127/0935-1221/2006/0018-0551

Atencio D., Andrade M.B., Christy A.G., Gieré R. & Kartashov P.M. 2010: The pyrochlore supergroup of minerals: nomenclature. *Can. Mineral.* 48, 673–698. https://doi.org/10.3749/canmin.48.3.673

Barrat J.A., Zanda B., Moynier F., Bollinger C., Liorzou C. & Bayon G. 2012: Geochemistry of CI chondrites: major and trace elements, and Cu and Zn isotopes. *Geochim. Cosmochim. Acta*. 83, 79–92. https://doi.org/10.1016/j.gca.2011.12.011

Borst A.M., Friis H., Andersen T., Nielsen T., Waight T.E. & Smit M.A. 2016: Zirconosilicates in the kakortokites of the Ilímaussaq complex, South Greenland: Implications for fluid evolution and high-field-strength and rare-earth element mineralization in agpaitic systems. *Mineral. Mag.* 80, 5–30. https://doi.org/10.1180/minmag.2016.080.046

Broska I., Vdovcová K., Konečný P., Siman P. & Lipka J. 2004: Accessory titanite in the granitoids of the Western Carpathians: distribution and composition. *Mineralia Slovaca* 36, 237–246 (in Slovak).

Brunarska I. & Anczkiewicz R. 2019: Geochronology and Sr–Nd–Hf isotope constraints on the petrogenesis of teschenites from the type-locality in the Outer Western Carpathians. *Geol. Carpath.* 70, 222–240. https://doi.org/10.2478/geoca-2019-0013

Cao M.J., Qin K.Z., Li G.M., Evans N.J. & Jin L.Y. 2015: In situ LA-(MC)-ICP-MS trace element and Nd isotopic compositions and genesis of polygenetic titanite from the Baogutu reduced porphyry Cu deposit,Western Junggar, NW China. *Ore Geol. Rev.* 65, 940–954. https://doi.org/10.1016/j.oregeorev.2014.07.014

Carlier G. & Lorand J.-P. 2008: Zr-rich accessory minerals (titanite, perrierite, zirconolite, baddeleyite) record strong oxidation associated with magma mixing in the south Peruvian potassic province. *Lithos* 104, 54–70. https://doi.org/10.1016/j.lithos.2007.11.008

Černý P. & Ercit T.S. 1989: Mineralogy of Niobium and Tantalum: crystal chemical relationships, paragenetic aspects and their economic implications. In: Möller P., Černý P. & Saupé F. (Eds.): Lanthanoides, Tantalum and Niobium. *Springer-Verlag,* Heidelberg, 27–79.

Černý P., Novák M. & Chapman R. 1995: The Al(Nb, Ta)Ti_{-2} substitution in titanite: the emergence of a new species? *Mineral. Petrol.* 52, 61–73. https://doi.org/10.1007/BF01163126

Chakhmouradian A.R. 2004: Crystal chemistry and paragenesis of compositionally unique (Al-, Fe-, Nb-, and Zr-rich) titanite from Afrikanda, Russia. *Am. Mineral*. 89, 1752–1762. https://doi.org/10.2138/am-2004-11-1222

Chakhmouradian A.R. & Mitchell R.H. 1999: Primary, agpaitic and deuteric stages in the evolution of accessory Sr, REE, Ba and Nb-mineralization in nepheline-syenite pegmatites at Pegmatite Peak, Bearpaw Mts, Montana. *Mineral. Petrol.* 67, 85–110. https://doi.org/10.1007/BF01165118

Chakhmouradian A.R., Reguir E.P. & Mitchell R.H. 2003: Titanite in carbonatitic rocks: genetic dualism and geochemical significance. *Periodico di Mineralogia* 72, 107–113.

Cherniak D.J. 2006: Zr diffusion in titanite. *Contrib. Mineral. Petrol.* 152, 639–647. https://doi.org/10.1007/s00410-006-0133-0

Clark A.M. 1974: A tantalum-rich variety of sphene. *Mineral. Mag.* 39, 605–607.

Crook W.W. & Oswald S.G. 1979: New data on cerian vesuvianite from San Benito County, California. *Am. Mineral.* 64, 367–368.

Dawson J.B., Smith J.V. & Steele I.M. 1995: Petrology and mineral chemistry of plutonic igneous xenoliths from the carbonatite volcano, Oldoinyo Lengai, Tanzania. *J. Petrol.* 36, 797–826. https://doi.org/10.1093/petrology/36.3.797

Della Ventura G., Bellatreccia F. & Williams C.T. 1999: Zr- and LREE-rich titanite from Tre Croci, Vico Volcanic complex (Latium, Italy). *Mineral. Mag.* 63, 123–130. https://doi.org/10.1180/002646199548240

Dolníček Z., Kropáč K., Uher P. & Polách M. 2010a: Mineralogical and geochemical evidence for multi-stage origin of mineral veins hosted by teschenites at Tichá, Outer Western Carpathians, Czech Republic. *Chem. Erde-Geochem.* 70, 267–282. https://doi.org/10.1016/j.chemer.2010.03.003

Dolníček Z., Urubek T. & Kropáč K. 2010b: Post-magmatic hydrothermal mineralization associated with Cretaceous picrite (Outer Western Carpathians, Czech Republic): interaction between host rock and externally derived fluid. *Geol. Carpath.* 61, 327–339. https://doi.org/10.2478/v10096-010-0019-y

Dolníček Z., Kropáč K., Janíčková K. & Urubek T. 2012: Diagenetic source of fluids causing the hydrothermal alteration of teschenites in the Silesian Unit, Outer Western Carpathians, Czech Republic: Petroleum-bearing vein mineralization from the Stříbrník site. *Mar. Petrol. Geol.* 37, 27–40. https://doi.org/10.1016/j.marpetgeo.2012.06.004

Dostal J. & Owen J.V. 1998: Cretaceous alkaline lamprophyres from northeastern Czech Republic: geochemistry and petrogenesis. *Geol. Rundsch.* 87, 67–77. https://doi.org/10.1007/s005310050190

Eliáš M. 1970: Lithology and sedimentology of the Silesian unit in the Moravskoslezské Beskydy Mts. *Sborn. Geol. Věd, Geol.* 18, 7–99 (in Czech).

Eliáš M., Skupien P. & Vašíček Z. 2003: A proposal for the modification of the lithostratigraphical division of the lower part of the Silesian Unit in the Czech area (Outer Western Carpathians). *Sbor. věd. Prací Vys. Šk. báň.-Techn. Univ., Ř. horn.-geol*. 49, 7–15 (in Czech).

Fitzgerald S., Leavens P.B., Rheingold A.L. & Nelen J.A. 1987: Crystal structure of a REE-bearing vesuvianite from San Benito County, California. *Am. Mineral.* 72, 625–628.

Froitzheim N., Plašienka D. & Schuster R. 2008: Alpine tectonics of the Alps and Western Carpathians. In: McCann T. (Ed.): Geology of Central Europe 2: Mesozoic and Cenozoic. *Bonn University,* Germany, 1141–1232.

Gadas P. 2012: A study of the granite-pegmatite system from ophiolites near Ruda nad Moravou. *Ph.D. Thesis, Faculty of Science, Masaryk University in Brno* (in Czech).

Gamble J.A. 1984: Petrology and geochemistry of differentiated teschenite intrusions from the Hunter Valley, New South Wales, Australia. *Contrib. Mineral. Petrol.* 88, 173–187. https://doi.org/10.1007/BF00371421

Gianetti B. & Luhr J.F. 1983: The white trachytic tuff of Roccamonfia Volcano (Roman region, Italy). *Contrib. Mineral. Petrol.* 84, 235–252. https://doi.org/10.1007/BF00371289

Gieré R. 1990: Hydrothermal mobility of Ti, Zr and REE: examples from the Bergell and Adamello contact aureoles (Italy). *Terra Nova* 2, 60–67. https://doi.org/10.1111/j.1365-3121.1990.tb00037.x

Gieré R. 1992: Compositional variation of metasomatic titanite from Adamello (Italy). *Schweiz. Mineral. Petrogr. Mitt.* 72, 167–177.

Green T.H. & Pearson N.J. 1986: Rare-earth element partitioning between sphene and coexisting silicate liquid at high pressure and temperature. *Chem. Geol.* 55, 105–119.

Grabowski J., Krzemiński L., Nescieruk P., Szydlo A., Paszkowski M., Pecskay Z. & Wójtowicz A. 2003: Geochronology of teschenitic intrusions in the Outer Western Carpathians of Poland–constraints from $^{40}K/^{40}Ar$ ages and biostratigraphy. *Geol. Carpath.* 54, 385–393.

Harangi S., Tonarini S., Vaselli O. & Manetti P. 2003: Geochemistry and petrogenesis of Early Cretaceous alkaline igneous rocks in Central Europe: implications for a long-lived EAR-type mantle component beneath Europe. *Acta Geol. Hung.* 46, 77–94.

Hayden L.A., Watson E.B. & Wark D.A. 2008: A thermobarometer for sphene (titanite). *Contrib. Mineral. Petrol.* 155, 529–540. https://doi.org/10.1007/s00410-007-0256-y

Himmelberg G.R. & Miller T.P 1980: Uranium- and thorium-rich vesuvianite from the Seward Peninsula, Alaska. *Am. Mineral.* 65, 1020–1025.

Hovorka D. & Spišiak J. 1988: Mesozoic Volcanism in the Western Carpathians. *Veda*, Bratislava, 1–263 (in Slovak).

Hu H., Li J.-W., McFarlane Ch.R.M., Luo Y. & McCarron T. 2017: Textures, trace element composition, and U–Pb ages of titanite from the Mangling granitoid pluton, East Qinling Orogen: Implication for magma mixing and destruction of the North China Craton. *Lithos* 284–285, 50–68. https://doi.org/10.1016/j.lithos.2017.03.025

Jiang S.-Y., Wang R.-Ch., Xu X.-S. & Zhao K.-D. 2005: Mobility of high field strength elements (HFSE) in magmatic-, metamorphic-, and submarine-hydrothermal systems. *Phys. Chem. Earth* 30, 1020–1029. https://doi.org/10.1016/j.pce.2004.11.004

Jiang P., Yang K.-F., Fan H.-R., Liu X., Cai Y.-Ch. & Yang Y.-H. 2016: Titanite-scale insights into multi-stage magma mixing in Early Cretaceous of NW Jiaodong terrane, North China Craton. *Lithos* 258–259, 197–214. https://doi.org/10.1016/j.lithos.2016.04.028

Jirásek J., Dolníček Z., Matýsek D. & Urubek T. 2017: Genetic aspects of barite mineralization associated with teschenite in the Silesian Unit, Outer Western Carpathians, Czech Republic. *Geol. Carpath.* 68, 119–129. https://doi.org/10.1515/geoca-2017-0010

Kapusta J. & Włodyka R. 1997: The X-ray powder diffraction profile analysis of analcimes from the teschenitic sills of the Outer Carpathians, Poland. *Neues Jahrb. Mineral., Monatshefte* 6, 241–255.

Keppler H. 1993: Influence of fluorine on the enrichment of high field strength trace elements in granitic rocks. *Contrib. Mineral. Petrol.* 114, 479–488. https://doi.org/10.1007/BF00321752

Kraynov S.R., Mer'kov A.N., Petrova N.G., Baturinskaya I.V. & Zharikova V.M. 1969: Highly alkaline (pH 12) fluosilicate waters in the deeper zones of the Lovozero massif. *Geochem. Int.* 6, 635–640.

Kropáč K., Dolníček Z., Buriánek D., Urubek T. & Mašek V. 2015: Carbonate inclusions in Lower Cretaceous picrites from the Hončova hůrka Hill (Czech Republic, Outer Western Carpathians): Evidence for primary magmatic carbonates? *Int. J. Earth Sci.* 104, 1299–1315. https://doi.org/10.1007/s00531-015-1152-8

Kropáč K., Dolníček Z., Uher P. & Urubek T. 2017: Fluorcaphite from hydrothermally altered teschenite at Tichá, Outer Western Carpathians, Czech Republic: compositional variations and origin. *Mineral. Mag.* 81, 1485–1501. https://doi.org/10.1180/minmag.2017.081.016

Kudělásková J. 1987: Petrology and geochemistry of selected rock types of teschenite association, Outer Western Carpathians. *Geol. Carpath.* 38, 545–573.

Kwak T.A.P. & Abeysinghe P.B. 1987: Rare earth and uranium minerals present as daughter crystals in fluid inclusions, Mary Kathleen U-REE skarn, Queensland, Australia. *Mineral. Mag.* 51, 665–670. https://doi.org/10.1180/minmag.1987.051.363.05

Kynický J., Xu Ch., Bajer A., Samec P. & Kynická A. 2009: New exploration of teschenite clan rocks: Sr and REE-rich fluorapatites. *Geol. Výzk. Mor. Slez.* 16, 66–69 (in Czech).

Lewandowski J.T., Pickering I.J. & Jacobson A.J. 1992: Hydrothermal synthesis of calcium - niobium and tantalum oxides with the pyrochlore structure. *Mater. Res. Bull.* 27, 981–988. https://doi.org/10.1016/0025-5408(92)90199-A

Liferovich R.P. & Mitchell R.H. 2005: Composition and paragenesis of Na-, Nb- and Zr-bearing titanite from Khibina, Russia, and crystal-structure data for synthetic analogues. *Can. Mineral.* 43, 795–812. https://doi.org/10.2113/gscanmin.43.2.795

Linnen R.L. & Keppler H. 2002: Melt composition control of Zr/Hf fractionation in magmatic processes. *Geochim. Cosmochim. Acta* 66, 3293–3301. https://doi.org/10.1016/S0016-7037(02)00924-9

Lucińska-Anczkiewicz A., Villa I.M., Anczkiewicz R. & Ślaczka A. 2002: $^{40}Ar/^{39}Ar$ dating of alkaline lamprophyres from the Polish Western Carpathians. *Geol. Carpath*. 53, 45–52.

Lumpkin G. & Mariano A. 1995: Natural occurrence and stability of pyrochlore in carbonatites, related hydrothermal systems, and weathering environments. *MRS Proceedings* 412, 831. https://doi.org/10.1557/PROC-412-831

Lyakhovich V.V. 1968: Accessory minerals. *Nauka*, Moscow, 1–276. (in Russian).

Mahmood A. 1973: Petrology of the teschenite rock series from the type area of Cieszyn (Teschen) in the Polish Carpathians. *Ann. Soc. Geol. Pol.* 43, 153–216.

Mandour M.A. 1982: Geochemical and Mineralogical Study of Rocks of Teschenite Association in the Sub-Beskydy Area (ČSSR). *MSc. Thesis, VŠB* Ostrava (in Czech).

Marks M.A.W. & Markl G. 2017: A global review on agpaitic rocks. *Earth Sci. Rev.* 173, 229–258. https://doi.org/10.1016/j.earscirev.2017.06.002

Matýsek D. 1989: Geochemical classification of rock of teschenite associaton. *Sbor. věd. Prací Vys. Šk. báň.-Techn. Univ., Ř. horn.-geol.* 35, 301–324 (in Czech).

Matýsek D. 1992: Contact metamorphism connected with the intrusion of teschenite association rocks in Krmelín locality, Northern Moravia, Czechoslovakia. *Acta Mus. Morav. Sci. Nat.* 77, 29–39 (in Czech).

Matýsek D. 2013: Evidence of rare earth elements (REE) mobilization in teschenites of the Beskydy Mts. region. *Acta Mus. Moraviae, Sci. geol.* 2, 101–113 (in Czech).

Matýsek D. & Jirásek J. 2016: Occurrences of slawsonite in rocks of the teschenite association in the Podbeskydí Piedmont area (Czech Republic) and their petrological significance. *Can. Mineral.* 54, 1129–1146. https://doi.org/10.3749/canmin.1500101

Matýsek D., Jirásek K., Skupien P. & Thomson S.N. 2018: The Žermanice sill: new insights into the mineralogy, petrology, age, and origin of the teschenite association rocks in the Western Carpathians, Czech Republic. *Int. J. Earth Sci.* 107, 2553–2574. https://doi.org/10.1007/s00531-018-1614-x

McLennan S.M. 1989: Rare earth elements in sedimentary rocks: influence of provenance and sedimentary processes. In: Lipin B.R. & McKay G.A. (Eds.): Geochemistry and mineralogy of rare earth elements. *Rev. Mineral.* 21, 169–200. https://doi.org/10.1515/9781501509032-010

McLeod G.W., Dempster T.J. & Faithfull J.W. 2011: Deciphering magma-mixing processes using zoned titanite from the Ross of Mull granite, Scotland. *J. Petrol.* 52, 55–82. https://doi.org/10.1093/petrology/egq071

Migdisov A.A. & Williams-Jones A.E. 2009: The stability of Zr in F-bearing hydrothermal solutions. *Geochim. Cosmochim. Acta* 73, A879.

Migdisov A.A., Williams-Jones A.E., van Hinsberg V. & Salvi S. 2011: An experimental study of the solubility of baddeleyite (ZrO_2) in fluoride-bearing solutions at elevated temperature. *Geochim. Cosmochim. Acta* 75, 7426–7434. https://doi.org/10.1016/j.gca.2011.09.043

Mitchell R.H. & Liferovich R.P. 2006: Subsolidus deuteric/hydrothermal alteration of eudialyte in lujavrite from Pilansberg alkaline complex, South Africa. *Lithos* 91, 352–372. https://doi.org/10.1016/j.lithos.2006.03.025

Monecke T., Kempe U., Monecke J., Sala M. & Wolf D. 2002: Tetrad effect in rare earth element distribution patterns: a method of quantification with application to rock and mineral samples from granite-related rare metal deposits. *Geochim. Cosmochim. Acta* 66, 1185–1196. https://doi.org/10.1016/S0016-7037(01)00849-3

Murdoch J. & Ingram B.L. 1966: A cerian vesuvianite from California. *Am. Mineral.* 51, 381–387.

Narebski W. 1990: Early rift stage in the evolution of western part of the Carpathians: geochemical evidence from limburgite and teschenite rock series. *Geol. Carpath.* 41, 521–528.

Njonfang E. & Nono A. 2003: Clinopyroxene from some felsic alkaline rocks of the Cameroon Line, Central Africa, petrological implications. *Eur. J. Mineral.* 15, 527–542. https://doi.org/10.1127/0935-1221/2003/0015-0527

Novák M. & Gadas P. 2010: Internal structure and mineralogy of a zoned anorthite-and grossular-bearing leucotonalitic pegmatite in serpentinized lherzolite at Ruda nad Moravou, Staré Město Unit, Czech Republic. *Can. Mineral.* 48, 629–650. https://doi.org/10.3749/CANMIN.48.3.629

O'Neill H.S.C. & Eggins S.M. 2002: The effect of melt composition on trace element partitioning: and experimental investigation of activity coefficients of FeO, NiO, CoO, MoO_2 and MoO_3 in silicate melts. *Chem. Geol.* 186, 151–181. https://doi.org/10.1016/S0009-2541(01)00414-4

Pacák O. 1926: Volcanic rocks at the northern foothill of the Moravské Beskydy Mts. *Česká Akad. Věd a Umění*, Praha, 1–232 (in Czech).

Pearce N.J.G. 1989: Zirconium-bearing amphiboles from the Igaliko dyke swarm, South Greenland. *Mineral. Mag.* 53, 107–110. https://doi.org/10.1180/minmag.1989.053.369.12

Perseil E.-A. & Smith D.C. 1995: Sb-rich titanite in the manganese concentrations at St. Marcel-Praborna, Aosta Valley, Italy: petrography and crystal-chemistry. *Mineral. Mag.* 59, 717–734. https://doi.org/10.1180/minmag.1995.059.397.13

Pieczka A., Hawthorne F.C., Ma C., Rossman G.R., Szełęg E., Szuszkiewicz A., Turniak K., Nejbert K., Ilnicki S.S., Buffat P. & Rutkowski B. 2017: Żabińskiite, ideally $Ca(Al_{0.5}Ta_{0.5})(SiO_4)O$, a new mineral of the titanite group from the Piława Górna pegmatite, the Góry Sowie Block, southwestern Poland. *Mineral. Mag.* 81, 591–610. https://doi.org/10.1180/minmag.2016.080.110

Plašienka D., Grecula P., Putiš M., Kováč M. & Hovorka D. 1997: Evolution and structure of the Western Carpathians: an overview. In: Grecula P., Hovorka D. & Putiš M. (Eds.): Geological Evolution of the Western Carpathians. *Miner. Slovaca – Monograph.*, Bratislava, 1–24.

Pouchou J. & Pichoir F. 1985: "PAP" procedure for improved quantitative microanalysis. *Microbeam Anal.* 20, 104–105.

Prowatke S. & Klemme S. 2005: Effect of melt composition on the partitioning of trace elements between titanite and silicate melt. *Geochim. Cosmochim. Acta* 69, 695–709. https://doi.org/10.1016/j.gca.2004.06.037

Prowatke S. & Klemme S. 2006: Rare earth element partitioning between titanite and silicate melts: Henry's law revisited. *Geochim. Cosmochim. Acta* 70, 4997–5012. https://doi.org/10.1016/j.gca.2006.07.016

Reguir E.P., Chakhmouradian A.R. & Evdokimov M.D. 1999: The mineralogy of a unique baratovite- and miserite-bearing quartz – albite – aegirine rock from the Dara-i-Pioz Complex, northern Tajikistan. *Can. Mineral.* 37, 1369–1384.

Ribbe P.H. 1980: Titanite. In: Ribbe P.H. (Ed.): Orthosilicates. *Reviews in Mineralogy* 5, *Mineralogical Society of America*, Washington, 137–154.

Rubin J.N., Henry C.D. & Price J.G. 1993: The mobility of zirconium and other "immobile" elements during hydrothermal alteration. *Chem. Geol.* 110, 137–154. https://doi.org/10.1016/0009-2541(93)90246-F

Sahama Th.G. 1946: On the chemistry of the mineral titanite. *Bull. Comm. Géol. Finlande* 24, 88–120.

Salvi S. & Williams-Jones A.E. 1996: The role of hydrothermal processes in concentrating high-field strength elements in the Strange Lake peralkaline complex, northeastern Canada. *Geochim. Cosmochim. Acta* 60, 1917–1932. https://doi.org/10.1016/0016-7037(96)00071-3

Salvi S. & Williams-Jones A.E. 2005: Alkaline granite-syenite deposits. In: Linnen R.L. & Samson I.M. (Eds.): Rare-Element Geochemistry and Mineral Deposits. *Short Course Notes – Geological Association of Canada* 17, 315–341.

Salvi S. & Williams-Jones A.E. 2006: Alteration, HFSE mineralisation and hydrocarbon formation in peralkaline igneous systems: Insights from the Strange Lake Pluton, Canada. *Lithos* 91, 19–34. https://doi.org/10.1016/j.lithos.2006.03.040

Salvi S., Fontan F., Monchoux P., Williams-Jones A.E. & Moine B. 2000: Hydrothermal mobilization of high field strength elements in alkaline igneous systems: Evidence from the Tamazeght Complex (Morocco). *Econ. Geol.* 95, 559–576. https://doi.org/10.2113/gsecongeo.95.3.559

Schosnig M., Hoffer E. & Usdowski H.E. 1994: Trace element partitioning between titanite, diopside and melt at 1 Atm. – an experimental study of system anorthite – diopside – titanite. *J. Czech Geol. Soc.* 39, 95–96.

Schuchová K. 2016: Petrographic variability of teschenites from Bludovice near Nový Jičín. *MSc Thesis, Faculty of Science, Palacký University Olomouc* (in Czech).

Schuchová K., Kropáč K., Dolníček Z. & Lehotský T. 2016: Petrographic variability of a body of teschenite from the site Bludovice near Nový Jičín (Silesian Unit, Outer Western Carpathians). *Geol. Výzk. Mor. Slez.* 23, 59–65 (in Czech).

Schwinn G. & Markl G. 2005: REE systematics in hydrothermal fluorite. *Chem. Geol.* 216, 225–248. https://doi.org/10.1016/j.chemgeo.2004.11.012

Seifert W. 2005: REE-, Zr-, and Th-rich titanite and associated accessory minerals from a kersantite in the Frankenwald, Germany. *Mineral. Petrol.* 84, 129–146. https://doi.org/10.1007/s00710-005-0076-6

Seifert W. & Kramer W. 2003: Accessory titanite: an important carrier of zirconium in lamprophyres. *Lithos* 71, 81–98. https://doi.org/10.1016/j.lithos.2003.07.002

Speer J.A. & Gibbs G.V. 1976: The structure of synthetic titanite, $CaTiOSiO_4$, and the domain textures of natural titanites. *Am. Mineral.* 61, 238–247.

Spišiak J. & Hovorka D. 1997: Petrology of the Western Carpathians Cretaceous primitive alkaline volcanics. *Geol. Carpath.* 48, 113–121 (in Slovak).

Šmíd B. 1978: The Investigation of Igneous Rocks of the Teschenite Association. *Manuscript, Central Geological Survey*, Prague, 1–153 (in Czech).

Smith A.L. 1970: Sphene, perovskite and coexisting Fe-Ti oxide minerals. *Am. Mineral.* 55, 264–269.

Smulikowski K. 1930: Les roches éruptives de la zone subbeskidique en Silésie et Moravie. *Kosmos* 54, 749–850 (in French).

Smulikowski K. 1980: Comments on the Cieszyn Magmatic Province (West Carpathian Flysch). *Ann. Soc. Geol. Pol.* 50, 41–54 (in Polish with English abstract).

Stepanov A.V., Bekenova G.K., Levin V.L. & Hawthorne F.C. 2012: Natrotitanite, ideally $(Na_{0.5}Y_{0.5})Ti(SiO_4)O$, a new mineral from the Verkhnee Espe deposit, Akjailyautas Mountains, Eastern Kazakhstan district, Kazakhstan: description and crystal structure. *Mineral. Mag.* 76, 37–44. https://doi.org/10.1180/minmag.2012.076.1.37

Storey C.D., Jeffries T.E. & Smith M. 2006: Common lead-corrected laser ablation ICP-MS U–Pb systematics and geochronology of titanite. *Chem. Geol.* 227, 37–52. https://doi.org/10.1016/j.chemgeo.2005.09.003

Stráník Z., Menčík E., Eliáš M. & Adámek J. 1993: Flysch belt of the West Carpathians, autochthonous Mesozoic and Paleogene in Moravia and Silesia. In: Přichystal A., Obstová V. & Suk M. (Eds.): Geology of Moravia and Silesia. *Moravské zemské muzeum a Sekce Geologických věd PřF MU*, 27–79 (in Czech).

Szopa K., Włodyka R. & Chew D. 2014: LA-ICP-MS U-Pb apatite dating of Lower Cretaceous rocks from teschenite-picrite association in the Silesian Unit (southern Poland). *Geol. Carpath.* 65, 273–284. https://doi.org/10.2478/geoca-2014-0018

Timofeev A. & Williams-Jones A.E. 2015: The origin of niobium and tantalum mineralization in the Nechalacho REE Deposit, NWT, Canada. *Econ. Geol.* 110, 1719–1735. https://doi.org/10.2113/econgeo.110.7.1719

Uher P., Broska I., Krzemińska E., Ondrejka M., Mikuš T. & Vaculovič T. 2019: Titanite composition and SHRIMP U–Pb dating as indicators of post-magmatic tectono-thermal activity: Variscan I-type tonalites to granodiorites, the Western Carpathians. *Geol. Carpath.* 70, 449–470. https://doi.org/10.2478/geoca-2019-0026

Urubek T., Dolníček Z., Kropáč K. & Lehotský T. 2013: Fluid inclusions and chemical composition of analcimes from Řepiště site (Outer Western Carpathians). *Geol. Výzk. Mor. Slez.* 20, 107–111 (in Czech).

Vlasov K.A., Sindeyeva N.D., Serdyuchenko D.P., Eshkova Je. M., Kuzmenko M.V. & Pyatenko Ju.A. 1964: Geochemistry, mineralogy and genetic types of rare-element deposits. Part II. Mineralogy of rare elements. *Nauka*, Moscow, 1–832. (in Russian).

Vuorinen J.H. & Hålenius U. 2005: Nb-, Zr- and LREE-rich titanite from the Alnö alkaline complex: Crystal chemistry and its importance as a petrogenetic indicator. *Lithos* 83, 128–142. https://doi.org/10.1016/j.lithos.2005.01.008

Watson E.B. 1979: Zircon saturation in felsic liquids: experimental results and applications to trace element geochemistry. *Contrib. Mineral. Petrol.* 70, 407–419.

Wieser T. 1971: Metamorphism of exo- and endocontacts of teschenites hosted by Flysch Carpathians in Poland. *Geol. Quarterly* 15, 901–922.

Wilkinson J.P.G. 1959: The geochemistry of a differentiated teschenite sill near Gunnedah, New South Wales. *Geochim. Cosmochim. Acta* 16, 123–150.

Włodyka R. 2007: The occurrence of Zr-bearing phases in the syenite rocks from the Polish Western Carpathians. *Miner. Polonica – Spec. Papers* 31, 303–306.

Włodyka R. & Karwowski Ł. 2003: A Mesozoic volcanic rock series in the Polish Western Carpathians. *Pol. Tow. Miner., Pr. Spec.* 22, 248–255.

Włodyka R. & Kozlowski A. 1997: Fluid inclusions in hydrothermal analcimes from the rocks of the Cieszyn magma province (Poland). In: ECROFI XIV Symposium, 350–351.

Wolf J.A. 1984: Variation in Nb/Ta during differentiation of phonolitic magma, Tenerife, Canary Islands. *Geochim. Cosmochim. Acta* 48, 1345–1348. https://doi.org/10.1016/0016-7037(84)90067-X

Woolley A.R., Platt R.G. & Eby N. 1992: Niobian titanite and eudialite from Ilomba nepheline syenite complex, north Malawi. *Mineral. Mag.* 56, 428–430. https://doi.org/10.1180/minmag.1992.056.384.19

Zabavnikova N.I. 1957: Isomorphic substitutions in sphene. *Geochemistry* 3, 271–278 (in Russian).

Zurevinski S.E. & Mitchell R.H. 2004: Extreme compositional variation of pyrochlore-group minerals at the Oka carbonatite complex, Quebec: evidence of magma mixing? *Can. Mineral.* 42, 1159–1168. https://doi.org/10.2113/gscanmin.42.4.1159